END

DATE
FILMED
7-77

MICROCOPY RESOLUTION TEST CHART

BRL

(12)

NW.

AD

MEMORANDUM REPORT NO. 2745

COMPARISON OF THEORETICAL AND MEASURED SIGNAL AND NOISE OUTPUTS OF A PASSIVE 35-GHz RADIOMETER

Orrin C. Kaste

April 1977

Approved for public release; distribution unlimited.

USA ARMAMENT RESEARCH AND DEVELOPMENT COMMAND
USA BALLISTIC RESEARCH LABORATORY
ABERDEEN PROVING GROUND, MARYLAND

The findings in this report are not to be construed as
an official Department of the Army position, unless
so designated by other authorized documents.

REPORT DOCUMENTATION PAGE		READ INSTRUCTIONS BEFORE COMPLETING FORM
1. REPORT NUMBER MEMORANDUM REPORT NO. 2745	2. GOVT ACCESSION NO.	3. RECIPIENT'S CATALOG NUMBER
4. TITLE *(and Subtitle)* COMPARISON OF THEORETICAL AND MEASURED SIGNAL AND NOISE OUTPUTS OF A PASSIVE 35-GHz RADIOMETER.		5. TYPE OF REPORT & PERIOD COVERED Final rept.,
		6. PERFORMING ORG. REPORT NUMBER
7. AUTHOR(s) ORRIN C. KASTE		8. CONTRACT OR GRANT NUMBER(s)
9. PERFORMING ORGANIZATION NAME AND ADDRESS US Army Ballistic Research Laboratory Aberdeen Proving Ground, Maryland 21005		10. PROGRAM ELEMENT, PROJECT, TASK AREA & WORK UNIT NUMBERS 1L662618AH80
11. CONTROLLING OFFICE NAME AND ADDRESS US Army Materiel Development & Readiness Command 5001 Eisenhower Avenue Alexandria, Virginia 22333		12. REPORT DATE APRIL 1977
		13. NUMBER OF PAGES 65
14. MONITORING AGENCY NAME & ADDRESS*(if different from Controlling Office)*		15. SECURITY CLASS. *(of this report)* Unclassified
		15a. DECLASSIFICATION/DOWNGRADING SCHEDULE

16. DISTRIBUTION STATEMENT *(of this Report)*

Approved for public release; distribution unlimited.

BRL-MR-2745

17. DISTRIBUTION STATEMENT *(of the abstract entered in Block 20, if different from Report)*

18. SUPPLEMENTARY NOTES

19. KEY WORDS *(Continue on reverse side if necessary and identify by block number)*

Passive Radiometer	Experimental Noise Output
Theoretical Signal Output	Signal-to-Noise Ratio
Experimental Signal Output	Sky Reflection Angle
Theoretical Noise Output	

20. ABSTRACT *(Continue on reverse side if necessary and identify by block number)* (kst)

Two expressions for calculating radiometer antenna temperature changes when a target is present are derived and compared favorably with a simple expression frequently used in the literature. One of the new expressions can be used to calculate the output signal pulse of a radiometer as it passes near or over a target, and can be used when the radiometer antenna axis is tilted from the vertical. Experimental data are compared with theoretical data; agreement is

(Continued on reverse side).

DD FORM 1473 EDITION OF 1 NOV 65 IS OBSOLETE

20. ABSTRACT (continued)

generally very good. A theoretical expression for the noise output of a radiometer was obtained from the literature. Values from this expression are found to be in good agreement with noise data obtained from laboratory and field measurements.

ACCESSION for

NTIS   White Section ☑
DDC   Buff Section   ☐
UNANNOUNCED   ☐
JUSTIFICATION

BY
DISTRIBUTION/AVAILABILITY CODES

DIST   AVAIL. and/or SPECIAL

TABLE OF CONTENTS

LIST OF ILLUSTRATIONS

I. INTRODUCTION

During the course of a brief study of the potential of using small passive radiometers for guiding fire-and-forget antitank missiles,[1] it became evident that significant improvements can be made to the simple theoretical model often used for the signal output of such radiometers. Since a radiometric measurement program was being completed at that time,[2] it was decided to pursue the matter further by comparing theoretical and experimental values of signal and noise outputs of a small, passive, 35-GHz radiometer.

This report presents derivations of two expressions for the signal output of a passive radiometer. The first expression is relatively simple and has somewhat restricted applicability. The second expression is much more general but it must be evaluated by numerical integration. Results obtained from these expressions are compared with measured data.

A theoretical expression for the noise output of a radiometer was obtained from the literature. Results from this expression are compared with noise data obtained from laboratory and field measurements. Finally, comparisons are made between calculated and experimentally determined signal-to-noise ratios.

II. THEORETICAL SIGNAL OUTPUT OF A PASSIVE RADIOMETER

An expression was derived for the peak signal output of a passive radiometer for the case when a target is present at the center of the antenna beam.[1] The derivation will be repeated in shortened form in order to provide continuity to the material presented here.

The radiant emittance of a black body is given by Planck's formula in general, but for the millimeter wavelength region of the spectrum the Rayleigh-Jeans approximation may be used. Thus,

$$N \approx \frac{2kT}{\lambda^2} ,$$

where k is Boltzmann's constant, T is the absolute temperature of the body and λ is the wavelength of the radiant emittance being considered.

---

[1] O.C. Kaste, "Consideration of Passive Radiometers for Guidance of Fire-and-Forget Antitank Missiles from the Viewpoint of Signal-to-Noise Ratio," BRL Memorandum Report No. 2489, June 1975. (AD #B004798L)

[2] K.A. Richer, "SADARM Millimeter Wave Radiometer Measurements," BRL Memorandum Report No. 2433, January 1975 (C). (AD #C001046L)

The units of N are power per unit frequency per unit projected area of the black body per unit solid angle $(\text{WHz}^{-1}\text{m}^{-2}\text{sr}^{-1})$. An antenna with a power gain pattern $G(\theta,\phi)$, and therefore a receiving cross section

$$A(\theta,\phi) = G(\theta,\phi) \frac{\lambda^2}{4\pi} \quad ,$$

will receive power in the amount of

$$\frac{1}{2} \cdot \frac{2k}{4\pi} \int_0^{2\pi} \int_0^\pi TG(\theta,\phi) \sin\theta d\theta d\phi \quad \text{WHz}^{-1}$$

from the radiating body (see Figure 1). The $\frac{1}{2}$ factor is present because an antenna responds to a single polarization. If the radiometer "sees" only a black body at a uniform temperature T, the expression reduces to

$$\frac{kT}{4\pi} \int_0^{2\pi} \int_0^\pi G(\theta,\phi) \sin\theta d\theta d\phi = kT \quad \text{WHz}^{-1}$$

since

$$\int_0^{2\pi} \int_0^\pi G(\theta,\phi) \sin\theta d\theta d\phi = 4\pi$$

from the definition of antenna gain. A radiometer having a bandwidth B will then receive kTB watts of power, assuming ideal response over the bandwidth. Since k and B are constants, the radiometer can be calibrated to indicate temperature.

In general, the radiometer will not be looking at black bodies, nor will T be uniform over all θ,ϕ. Nevertheless, the radiometer can be calibrated using a black body at known temperature, and it will then indicate equivalent black body or radiometric temperatures based on the power it receives when looking at a real-world scene. Expressed mathematically,

$$T_A = \frac{1}{4\pi} \int_0^{2\pi} \int_0^\pi T(\theta,\phi)G(\theta,\phi) \sin\theta d\theta d\phi \quad ,$$

8
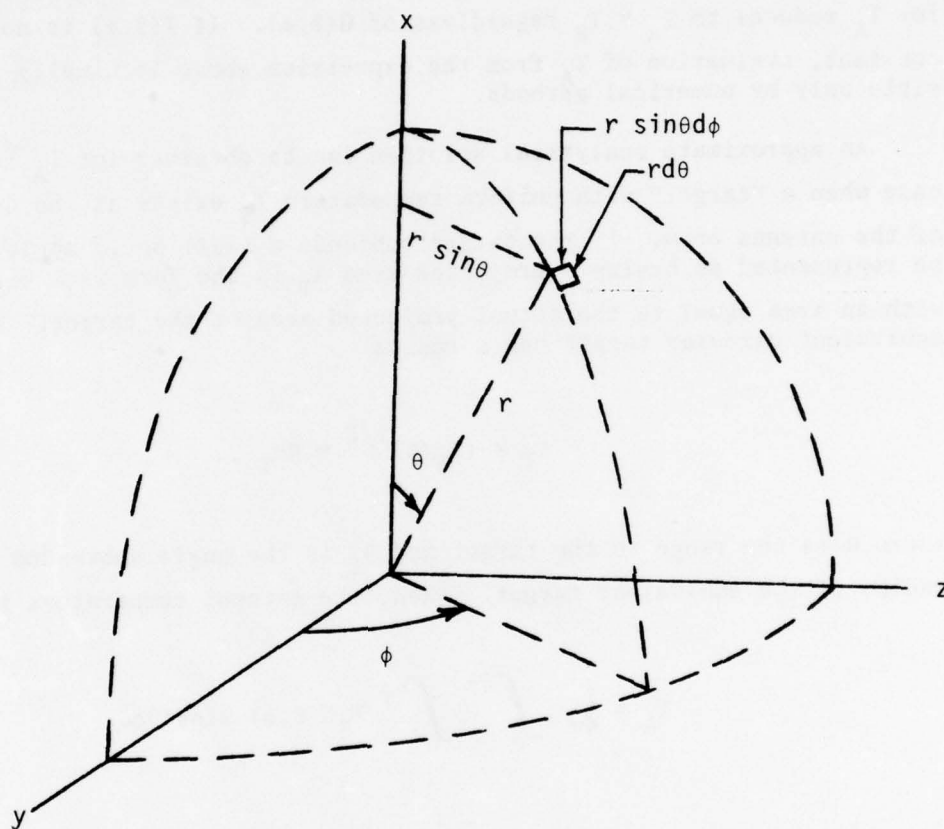
Figure 1. Elemental Projected Area Seen by Antenna
in Direction θ,φ (Antenna axis along x-axis).

9

where T_A is the indicated radiometric temperature or, as it is often called, the antenna temperature, and $T(\theta,\phi)$ is the radiometric temperature in direction θ,ϕ. If $T(\theta,\phi)$ is a constant, T_B, the expression for T_A reduces to $T_A = T_B$ regardless of $G(\theta,\phi)$. If $T(\theta,\phi)$ is not a constant, evaluation of T_A from the expression above is usually possible only by numerical methods.

An approximate analytical solution can be obtained for T_A for the case when a "target" with uniform temperature T_T exists at the center of the antenna beam. If the target subtends a small solid angle it may be represented as having a projected area A_T in the form of a circle with an area equal to the actual projected area of the target. The equivalent circular target has a radius

$$r_T = (A_T/\pi)^{1/2} \approx R\theta_T ,$$

where R is the range to the target and θ_T is the angle subtended by the radius of the equivalent target. Then, the antenna temperature is

$$T_A = \frac{1}{4\pi} \int_0^{2\pi} \int_0^{\theta_T} T_T G(\theta,\phi) \sin\theta d\theta d\phi$$

$$+ \frac{1}{4\pi} \int_0^{2\pi} \int_{\theta_T}^{\pi} T(\theta,\phi) G(\theta,\phi) \sin\theta d\theta d\phi .$$

If it is assumed that the area behind the target (i.e., the portion of the scene hidden from the radiometer antenna because the target is present) has a constant radiometric temperature T_{BT}, the expression for T_A can be written as

$$T_A = \frac{1}{4\pi} \int_0^{2\pi} \int_0^{\theta_T} T_T G(\theta,\phi) \sin\theta d\theta d\phi$$

$$+ \frac{1}{4\pi} \int_o^{2\pi} \int_o^\pi T(\theta,\phi)G(\theta,\phi) \sin\theta d\theta d\phi$$

$$- \frac{1}{4\pi} \int_o^{2\pi} \int_o^{\theta_T} T_{BT}G(\theta,\phi) \sin\theta d\theta d\phi .$$

Now, a good approximation for the power pattern of a radiometer antenna (especially near the center of the beam) is

$$G(\theta,\phi) = G_o e^{-b\theta^2} ,$$

as was established by Patton and Wilson.[3] In this expression G_o is the antenna power gain at the center of the beam, and b is a constant which characterizes the antenna pattern. The 3-db beamwidth (total angle) of this pattern is given by $\theta_{3db} = 2(\ell n2/b)^{1/2}$ rad. Then, since θ_T is assumed to be small, $\sin\theta \approx \theta$ for $\theta \leq \theta_T$, and

$$T_A \approx \frac{1}{4\pi} \int_o^{2\pi} \int_o^{\theta_T} (T_T - T_{BT})G_o e^{-b\theta^2} \theta d\theta d\phi$$

$$+ \frac{1}{4\pi} \int_o^{2\pi} \int_o^\pi T(\theta,\phi)G(\theta,\phi) \sin\theta d\theta d\phi$$

The first term is easily integrated to yield

$$\left(\frac{T_T - T_{BT}}{4b}\right) G_o \left(1 - e^{-b\theta_T^2}\right) .$$

---

[3] R.B. Patton, Jr. and C.L. Wilson, "The VARR Method, A Technique for Determining the Effective Power Patterns of Millimeter-Wave Radiometric Antennas," BRL Report No. 1322, May 1966. (AD #640009)

11

The second term cannot be integrated unless T and G are defined. (Note that G has been left in general form because the range of integration on θ is not small in this term.) However, this term is the expression for the radiometric temperature of the scene without the target. Let this temperature be designated T_s. Then,

$$T_A \approx \frac{(T_T - T_{BT})G_o}{4b} (1 - e^{-b\theta_T^2}) + T_s \ .$$

This expression can be simplified by utilizing the relationship

$$\int_0^{2\pi} \int_0^{\pi} G(\theta, \phi) \ \sin\theta d\theta d\phi = 4\pi \ ,$$

which for a symmetrical antenna beam, i.e., one where G is only a function of θ, reduces to

$$\int_0^{\pi} G(\theta) \ \sin\theta d\theta = 2 \ .$$

For $G(\theta) = G_o e^{-b\theta^2}$ as assumed above, and with b quite large (e.g., 400) so as to produce a narrow beam, it can be shown by numerical integration (see Reference 1) that satisfaction of the above relationship requires $G_o = 4b$. The expression for T_A then is

$$T_A \approx (T_T - T_{BT})(1-e^{-b\theta_T^2}) + T_s \ .$$

Introducing the notation

$$\Delta T_A = T_A - T_s \text{ and } \Delta T_T = T_T - T_{BT} \ ,$$

we have

$$\Delta T_A \approx \Delta T_T(1-e^{-b\theta_T^2}) \ .$$

12

In words, the change in antenna temperature resulting from the presence of a target in the antenna beam is equal to the difference between the radiometric temperatures of the target and its background times a function of the antenna beamwidth and the subtended angle of the target.

The expression above can be written in terms of the target area A_T, and the range R to the target:

$$\Delta T_A / \Delta T_T \approx [1 - \exp{(-bA_T/\pi R^2)}].$$

Figure 2 shows a plot of this expression as a function of R for b = 400 and A_T = 15 m^2. (With b = 400, the 3-db beamwidth of the antenna is 4.8 deg.) The drastic reduction in $\Delta T_A / \Delta T_T$ with increasing range is very obvious. It should be noted that no allowance has been made for effects of the atmosphere on the radiation received by the radiometer. These effects are not significant for the ranges shown in Figure 2, especially at 35 GHz. At greater ranges and for other frequencies the effects can be quite large.

The expression derived above yields satisfactory results for ΔT_A for targets which appear roughly circular as viewed by the radiometer. The results tend to be more valid at longer ranges than at very short ranges. Also, the results are valid only for the target centered in the antenna beam. To overcome these model deficiencies an alternate improved expression was developed for ΔT_A as described below.

Consider the situation depicted in Figure 3. Here the radiometer antenna is at altitude H (above flat terrain) and its axis of symmetry is at an angle θ_F from the vertical. This angle lies in the y-z plane of a Cartesian coordinate system centered at the ground directly beneath the antenna. A target with temperature contrast ΔT_T has an elemental area dxdy at x,y in the ground plane. It is assumed that the target appears two-dimensional to the radiometer. The situation described corresponds to a radiometer measurement setup for the SADARM (Sense and Destroy Armor) project (Reference 2).

The slant range from the antenna to area dxdy is $(H^2+x^2+y^2)^{1/2}$ and thus the antenna receiving solid angle relative to point (x,y) is

$$\frac{G(H, \theta_F, x,y)\lambda^2}{4\pi(H^2+x^2+y^2)} ,$$

13

$A_T = 15$ m^2

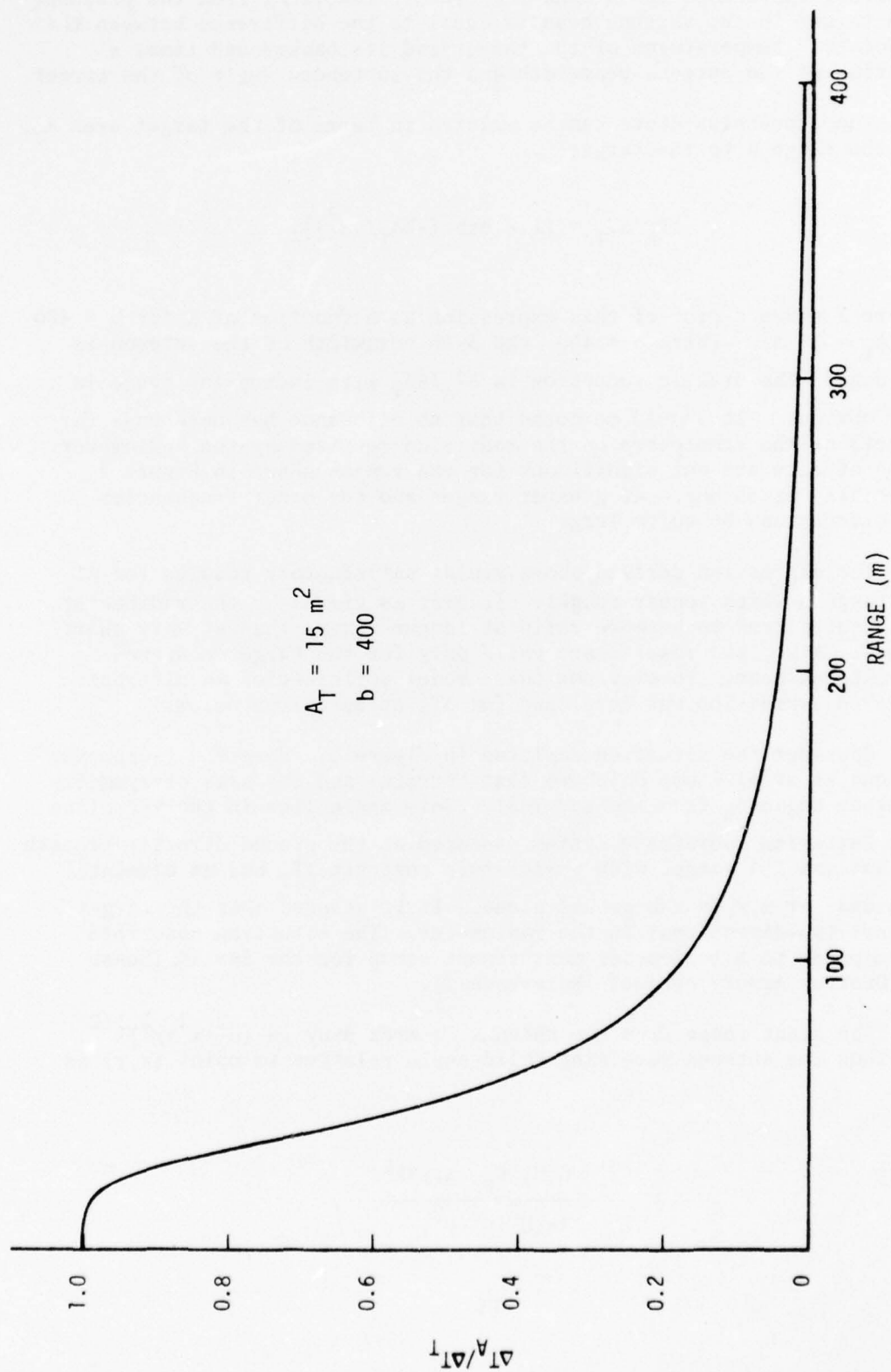$b = 400$

RANGE (m)

$\Delta T_A / \Delta T_T$

Figure 2. Normalized Antenna Temperature Change as a Function of Range
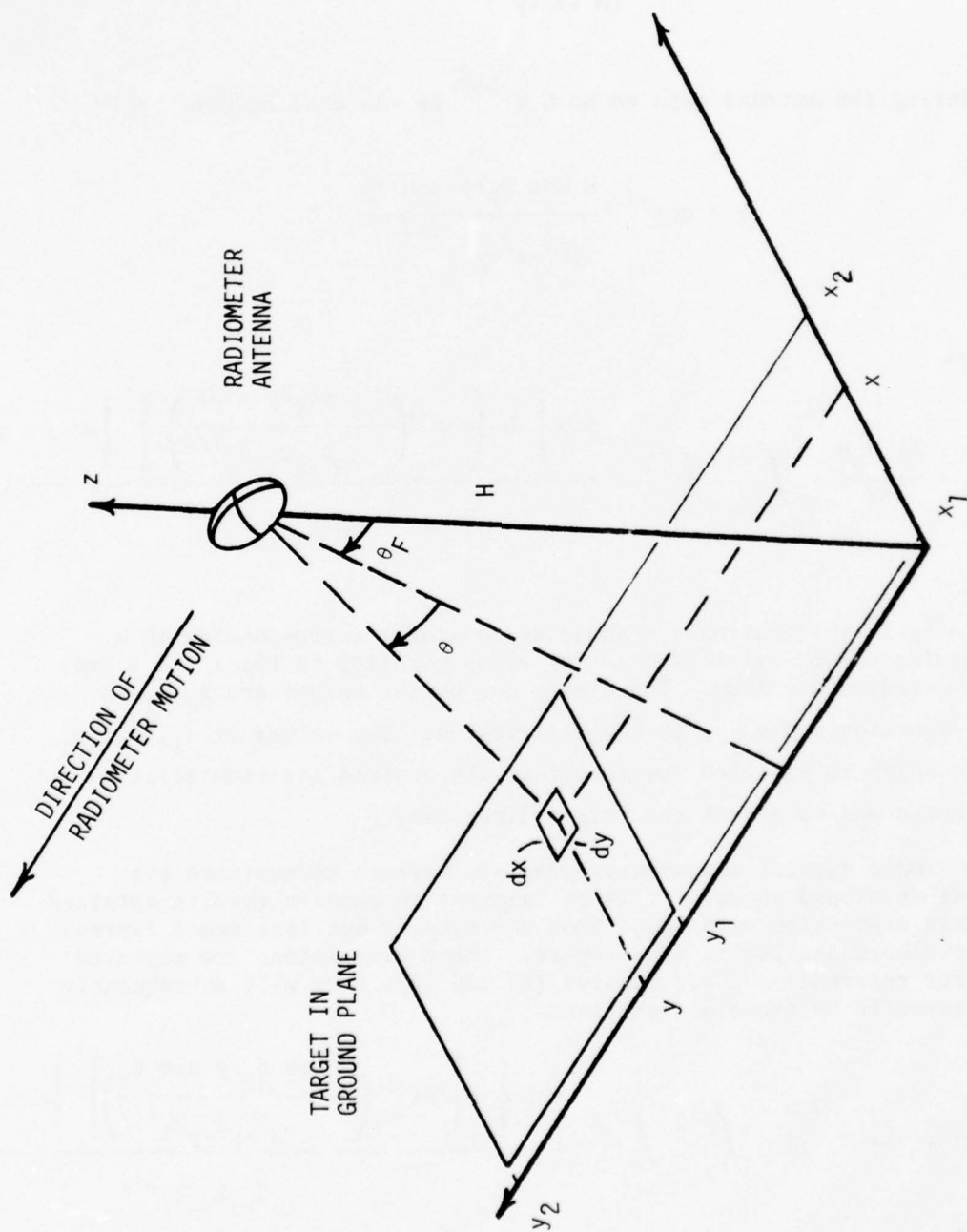
Figure 3. Radiometer-Target Geometry

where G is the antenna power gain in the direction of area dxdy. The projected area of dxdy, i.e., the area "seen" by the antenna, is

$$\frac{dxdy \, H}{(H^2+x^2+y^2)^{1/2}} \quad .$$

Considering the antenna gain to be $G_o e^{-b\theta^2}$ as was done before, where

$$\theta = \cos^{-1} \frac{H \cos \theta_F + y \sin \theta_F}{(H^2+x^2+y^2)^{1/2}} \quad ,$$

we have

$$\Delta T_A = \frac{\Delta T_T G_o H}{4\pi} \int_{y_1}^{y_2} \int_{x_1}^{x_2} \frac{\exp\left\{ -b \left[\cos^{-1}\left(\frac{H \cos\theta_F + y \sin\theta_F}{(H^2+x^2+y^2)^{1/2}} \right) \right]^2 \right\} dxdy}{(H^2+x^2+y^2)^{3/2}} \quad .$$

The limits of integration are shown as constants corresponding to a rectangular target oriented with its sides parallel to the x and y axes of the coordinate system. The dimensions of the target are x_2-x_1 in the x-direction and y_2-y_1 in the y-direction. The values of x_1, x_2, y_1, y_2 are chosen to position the target at the desired location relative to the antenna and to select the target dimensions.

A simple digital computer program was written to evaluate the integral developed above. It is of interest to compare results obtained from this expression with those from the simpler but less exact expression developed earlier in this report. These expressions are repeated below for reference and are labeled (A) and (B); they will subsequently be referred to by these designations.

$$(A) \quad \Delta T_A / \Delta T_T = \frac{G_o H}{4\pi} \int_{y_1}^{y_2} \int_{x_1}^{x_2} \frac{\exp\left\{ -b \left[\cos^{-1}\left(\frac{H \cos \theta_F + y \sin \theta_F}{(H^2+x^2+y^2)^{1/2}} \right) \right]^2 \right\} dxdy}{(H^2+x^2+y^2)^{3/2}} \quad .$$

(B) $\quad \Delta T_A / \Delta T_T = 1 - \exp(-bA_T / \pi R^2)$

Table I compares $\Delta T_A / \Delta T_T$ as calculated from (A) and (B) for parameter values as shown.

TABLE I

$b = 400$	$A_T = 15 \text{ m}^2$	$x_1 = -2.5 \text{ m}$
$G_o = 1600$	$y_1 = -1.5 \text{ m}$	$x_2 = 2.5 \text{ m}$
$\theta_F = 0$	$y_2 = 1.5 \text{ m}$	

	$\Delta T_A / \Delta T_T$		
$R(= H)$	(A)	(B)	(C)
10 m	1.000⁻	1.000⁻	(27.55)
30	0.828	0.880	(3.06)
50	0.510	0.534	(1.10)
70	0.314	0.323	0.562
100	0.171	0.174	0.276
200	0.046	0.047	0.069
300	0.021	0.021	0.031
500	0.008	0.008	0.011

Agreement between (A) and (B) is very good for ranges greater than 100 m and fairly good for ranges of 30-70 m. For targets departing further from a circular shape the agreement between expressions (A) and (B) would not be so good. For example, for a target of dimensions 1 by 15 m, expression (A) gives a value of 0.223 at R = 50 m, compared with the value of 0.534 for expression (B).

A commonly used expression for calculation of $\Delta T_A/\Delta T_T$ is based on the concept that $\Delta T_A/\Delta T_T$ will be equal to the ratio of the target area to the antenna beam area at the target range. The 3-db beamwidth is usually used to define the beam area. Thus

$$(C) \qquad \Delta T_A/\Delta T_T \approx \frac{4A_T}{\pi(R\theta_{3db})^2} = \frac{A_T b}{\pi R^2 \ln 2}$$

for the antenna pattern assumed above. Values computed from this expression are also given in Table I. The results from (C) are quite optimistic at all ranges. For short ranges expression (C) obviously breaks down because the target area exceeds that of the 3-db beam. These erroneous results are shown in parentheses.

The optimism of (C) at longer ranges arises from the use of the 3-db beamwidth to define the beam area. It is assumed that the target is at the center of the beam and is small enough that the gain of the beam over the entire target is equal to the peak gain. The area of the beam to be used in (C) then should be such that the solid angle of the equivalent beam times the peak gain is equal to the total power of the actual beam. For the antenna pattern used ($G_o e^{-b\theta^2}$) the 3-db beamwidth is $2\sqrt{\ln 2/b}$ rad. At range R the projected area covered by the 3-db beam is therefore

$$\frac{\pi}{4} R^2 \left(2\sqrt{\ln 2/b}\right)^2 = \pi R^2 \ln 2/b \ .$$

With a gain of $G_o = 4b$ over the entire solid angle of $\pi \ln 2/b$ sr, the total power would be $4\pi \ln 2$. The actual value should be 4π from general antenna theory. Thus the beamwidth used in calculating the area of the antenna beam for expression (C) should be

$$\theta_{3db}\Big/\sqrt{\ln 2} \ .$$

Then,

$$(C)' \qquad \Delta T_A/\Delta T_T = \frac{4A_T \ln 2}{\pi(R\theta_{3db})^2} = \frac{A_T b}{\pi R^2} \ .$$

18

Values calculated from this expression are listed below.

R	(C)'
10 m	(19.1)
30	(2.12)
50	0.764
70	0.390
100	0.191
200	0.048
300	0.021
500	0.008

These values of $\Delta T_A/\Delta T_T$ agree quite well with those from expressions (A) and (B), for R greater than 100 m. As before, the expression breaks down for very short ranges.

All of the above calculations of ΔT_A are based on the target being at the center of the antenna beam. Expression (A) is the only one which can be used to calculate $\Delta T_A/\Delta T_T$ for the target not at the center of the beam. For example, for a 3 by 5 metre target, the value of $\Delta T_A/\Delta T_T$ at a range of 30 m is 0.828 with the beam centered on the target. With the beam centered on a short edge of the target the value drops to 0.422, and with the beam centered on a corner of the target the value is only 0.249. At greater ranges the reduction of $\Delta T_A/\Delta T_T$ resulting from the beam not pointing exactly at the center of the target is less pronounced than at short ranges. At 100 m, the center, edge, and corner values of $\Delta T_A/\Delta T_T$ are 0.171, 0.138, and 0.127 respectively. For ranges greater than 400 m the center, edge, and corner values of $\Delta T_A/\Delta T_T$ are essentially equal.

Expression (A) can be used to calculate the "signal pulse" of a radiometer as it passes over a target; the passage is simulated by choosing an appropriate succession of values for y_1 and y_2. The signal pulse shows the rise and fall of ΔT_A as a function of radiometer position with respect to the target. Examples are shown in Figures 4 and 5. Figure 4 shows calculated results for the case when the radiometer is looking straight
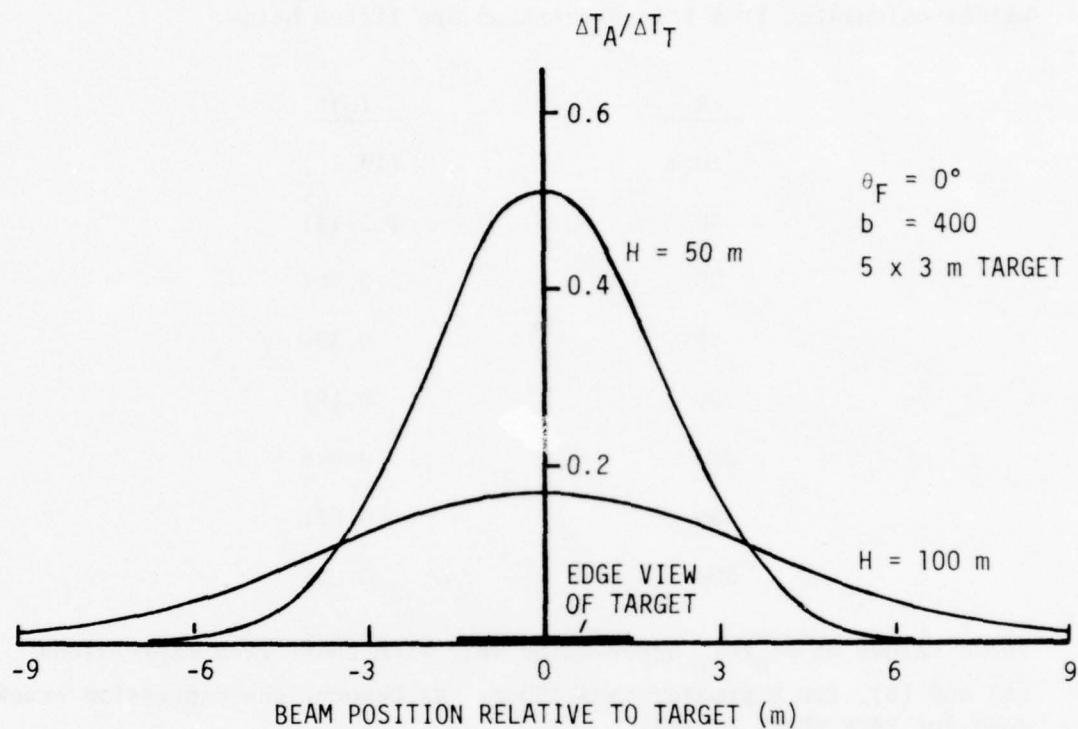
19

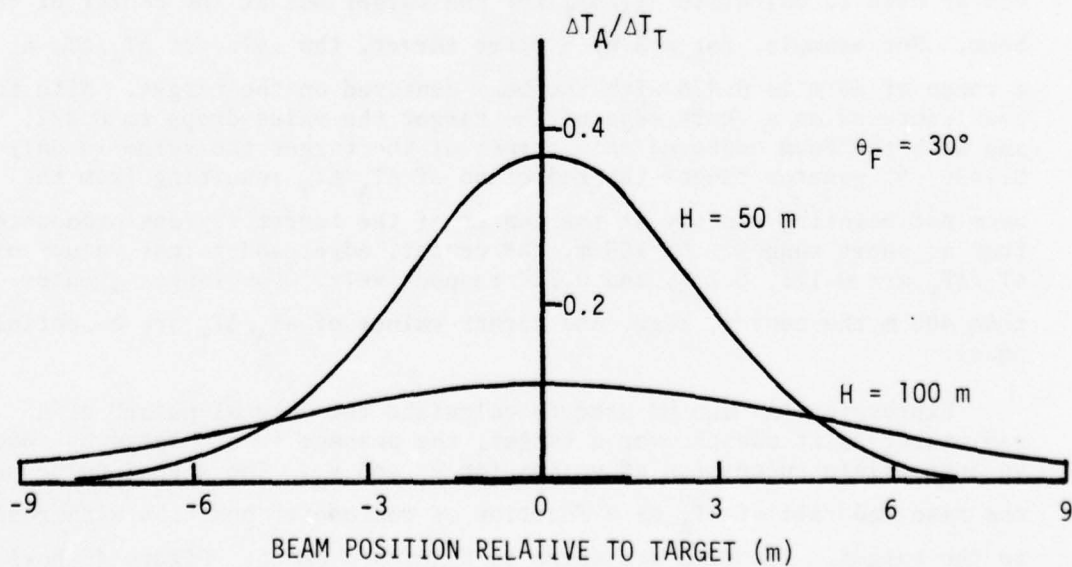Figure 4. Normalized Radiometer Signal Pulses ($\theta_F = 0°$)

Figure 5. Normalized Radiometer Signal Pulses ($\theta_F = 30°$)

20

down as it passes over a target from left to right; the radiometer moves parallel to the shorter edges of the target and passes over the center of the target. When the radiometer is directly over the target at an altitude of 50 m, the value of $\Delta T_A/\Delta T_T$ is 0.51; when the radiometer is over a long edge of the target, $\Delta T_A/\Delta T_T$ is 0.38. When the altitude is increased to 100 m, the signal pulse becomes lower and broader, reaching a peak value of only 0.17.

Figure 5 shows signal pulses for the same situations as were de-scribed for Figure 4, except the radiometer antenna is tilted 30° forward from the vertical. The abscissa in Figure 5 corresponds to the position of the center of the antenna beam on the ground. The radiometer now sees the target at a slant-range which is greater than the altitude, and also sees a projected area smaller than the actual target area. Consequently the signal pulses are substantially lower in amplitude than when the radiometer is looking straight down. A further result of the tilted antenna is the asymmetry of the signal pulse discernible on close inspection of Figure 5.

III. THEORETICAL NOISE OUTPUT OF A PASSIVE RADIOMETER

The radiometer under consideration here is of the full-power passive type. Taylor conducted a detailed review[4] of expressions for the sensi-tivity of passive radiometers. His expression for the root-mean-square noise output of a full-power radiometer is

$$\Delta T_{rms} = \frac{\sqrt{\pi}\ [(F-1)T_o + T_A]}{2\sqrt{B\tau}}\ ,$$

where F is the radiometer noise figure based on a reference temperature T_o, and T_A is the antenna temperature. The predetection bandwidth of the radiometer is B Hz, and the postdetection filter has a time constant of τ seconds.

The reference temperature T_o is usually 290 K (or 300 K), and the antenna temperature T_A is typically about 260 K when the antenna is pointed at terrain. With these values, the noise output given by the expression above is as shown on Figure 6, where ΔT_{rms} is plotted versus F for two values of Bτ. Since F values of about 4 are attainable for small 35-GHz radiometers, the noise output can be made less than 1 K by making Bτ larger than 10^6.

---

[4] H.P. Taylor, "The Radiometer Equation," The Microwave Journal, May 1967, pp. 39-42.
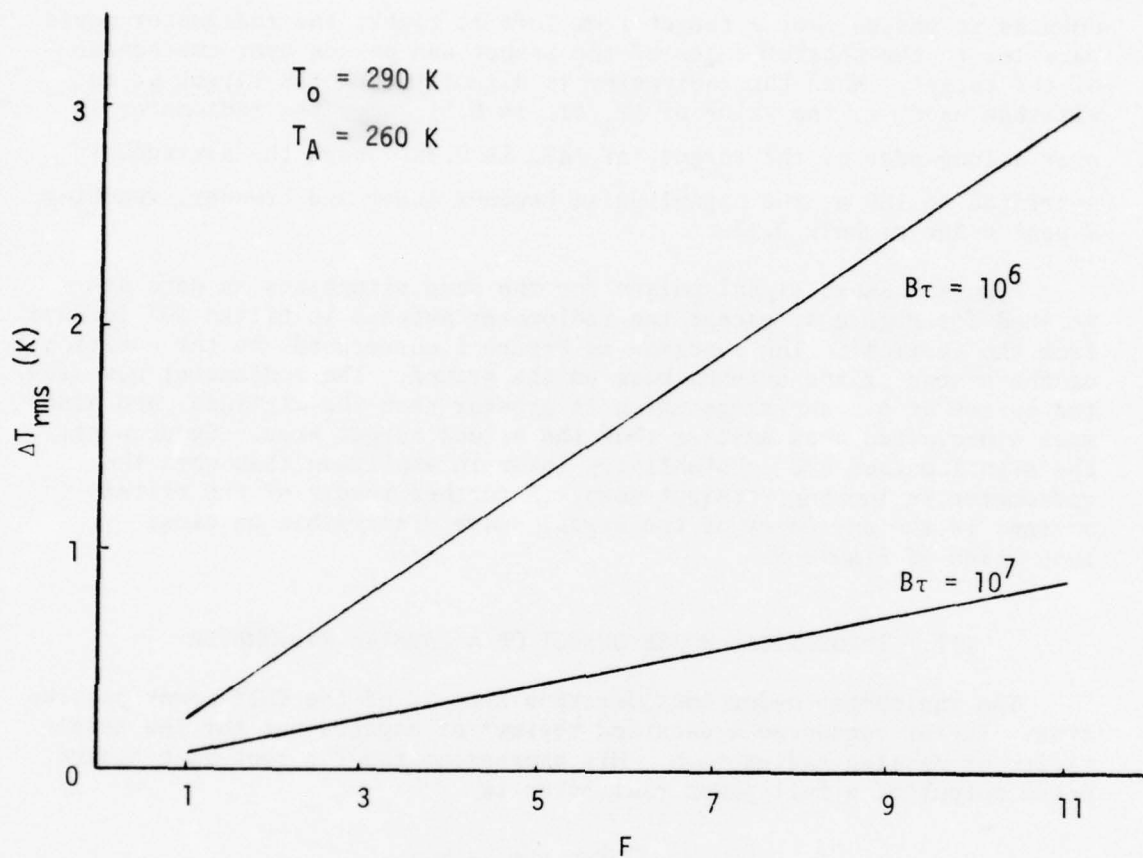
21

Figure 6. Radiometer Noise Output vs Noise Figure

IV. COMPARISON OF THEORETICAL AND EXPERIMENTAL RESULTS

Measurements made at BRL for the SADARM Program provided a good source of passive radiometer test results for comparison with results based on theoretical calculations. Data obtained from 26 passes of a helicopter-borne 35-GHz radiometer over a square metal sheet 3.66 m on a side, at altitudes ranging from about 30 to 150 metres, are presented in tabular form in Appendix A. These data were used to determine a value of b for the parabolic reflector antenna which was used during the runs. A value of 370 was established by an analysis described in Appendix B. The calculated 3-db beamwidth of the antenna beam is then

$$2 \times (\ln 2/b)^{1/2} = 0.0866 \text{ rad } (4.96°)$$

based on the model used in this report.

Using $b = 370$, $\Delta T_T = 250$ K (see Appendix B) and an antenna tilt angle $\theta_F = \pi/6$ rad, with a 3.66 x 3.66 m target, the predicted peak values of ΔT_A versus altitude as determined from expression (A) in Section II are plotted on Figure 7. Three curves are shown, the first for the antenna pointing directly at the center of the target, the second for the antenna pointing at the midpoint of one of the side edges of the target (1.83 m from the target center) and the third for the antenna beam centered along the fore-aft dimension of the target but 0.91 m off the target (2.74 m from the target center). The calculated curves converge as the altitude of the antenna increases, but for altitudes below about 75 m the value of ΔT_A is quite sensitive to antenna position relative to the target. For example, at an altitude of 30 m the calculated values of ΔT_A for three positions of the antenna are as follows:

Antenna Position	Peak ΔT_A
On target center	167 K
On target edge	98 K
Off target (0.91 m beyond edge)	46 K

Also shown on Figure 7 are experimental data points. These data were obtained from radiometer measurements described briefly in Appendix A and more fully in a report by Richer (Reference 2). The experimental points have been placed in four groups. The first group, represented by
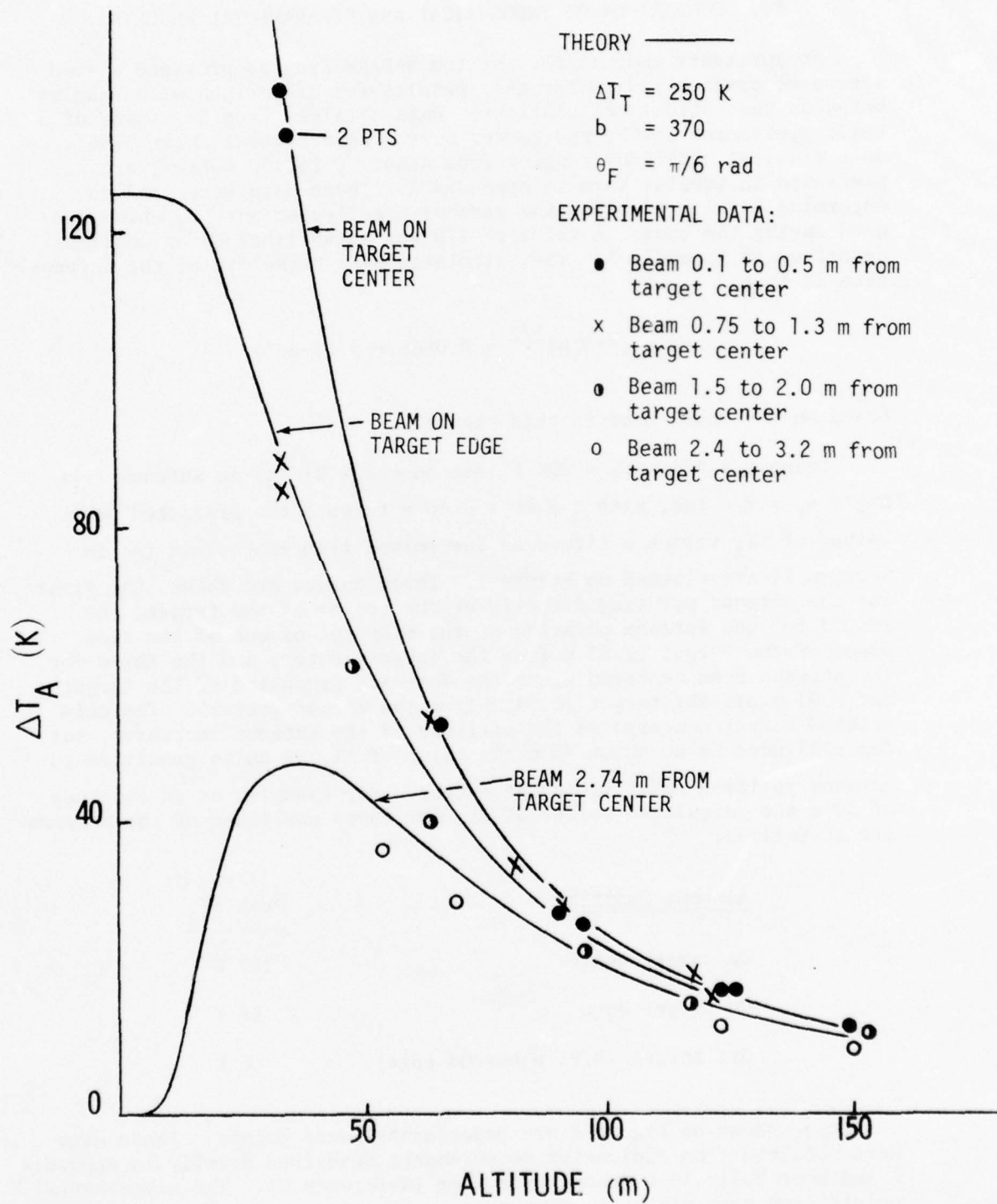
23

Figure 7. Peak Antenna Temperature Change vs Altitude

24

the solid dots, consists of peak readings of incremental antenna temperature for flights where the antenna beam passed almost directly over the center of the target. The agreement with the corresponding theoretical curve is very close over the range of altitudes included in the measurement program.

The second group of data points, represented by x's, consists of peak readings for flights when the beam passed 0.75 to 1.3 m to the right or left of target center. These points should lie between the upper two curves on the figure, and most of the points are in this region or close to it. The two points obtained when the altitude was 34 m are somewhat lower than corresponding theoretical values, for unknown reasons.

The third group of data points, represented by half-filled dots, consists of peak readings for flights where the beam passed 1.5 to 2.0 m from target center (roughly over the edge of the target). These points agree quite well with the theoretical curve, although they tend to be a little lower.

The fourth group, represented by open dots, consists of peak readings for flights where the beam passed 2.4 to 3.2 m from target center. Again, agreement with theory is good, with the experimental points falling a bit lower.

The generally good agreement between theory and experiment appears to confirm the basic validity of the model which was derived. Refinements of the model are possible, of course. The fact that the experimental data are lower than theoretical values when the antenna beam is not centered on the target may indicate that the off-axis representation of the theoretical beam pattern could be improved. The effect of the atmosphere on the radiometric signal could be included, but as mentioned previously, the effect is negligible (0.1 db/km) for 35-GHz radiometers at short ranges. Another consideration is the reflection angle of the target. For a radiometer looking nearly straight down, the sheet metal target appears to be essentially at the temperature of the zenith sky. However, when the radiometer antenna axis is not perpendicular to the target, the reflected temperature is from a part of the sky not directly overhead. Since the sky temperature is higher away from zenith, it follows that the radiometer reading will be affected. A brief investigation was made of the influence of off-zenith sky temperatures on the theoretical radiometric readings. Since the apparent sky temperature at 35 GHz does not increase much until the zenith angle exceeds roughly 40°, it was not expected that the influence would be significant for the situation treated in this report. This was confirmed by the analysis which is presented in Appendix C.

Further evidence of the agreement between theory and experiment is obtained by comparing calculated and measured radiometer signal pulses. These pulses show the change in temperature indicated by the radiometer as it passes over a target. The change in temperature is a function of

the relative position of the radiometer with respect to the target. In the SADARM measurements the radiometer was carried by a helicopter at a fairly uniform rate, and thus the signal pulse can be plotted as a function of time. For the 26 March 1974 runs the helicopter speed was nominally 36 m/s (70 knots). At this speed the 3.66-m target would be crossed in 0.10 seconds, and this value has been used in plotting the signal pulses. (Spot checks of video tapes revealed that the 103.6-m distance between the sheet metal target and a tank target was covered in 2.76 and 2.87 seconds in runs 23 and 26, respectively, for average speeds of 37.5 and 36.1 m/s. Attempts were made to determine the time to cross the sheet metal target, but video picture quality and the effects of helicopter oscillations precluded making accurate readings over the short intervals of time involved. Typical apparent values of slightly more than 0.1 second were observed.) Figures 8 through 12 show theoretical (solid line) and experimental (points) results for four different situations as given below.

Figure	ALT	Position of Beam Relative to Target Center Line	Measurement Run No.
8	123 m	0.1 m right	11
9	91	1.1 m left	17
10	69	2.6 m left	23
11	34	0.1 m left	26
12	34	1.3 m left	25

The time on the abscissa of each plot is relative to the time when the antenna beam axis is centered along the fore-aft dimension of the target. Experimental data were available in digitized form at 0.01-second intervals; these points have been plotted without attempting to draw a curve through them. The reference value of the antenna temperature (e.g., 258 K on Figure 8) from which ΔT_A was measured is the scene temperature without the target as described and tabulated in Appendix A. The signal pulses are shown with negative values since the target is colder than the background terrain and the antenna temperature decreases as the radiometer passes over.

Figure 8 shows results for the situation when the radiometer was carried at an altitude of 123 m above ground and nearly over the center of the target. Agreement between theory and experiment is very good although the experimental values fall off slightly faster than the theoretical curve. The experimental points show some evidence of pitch

26

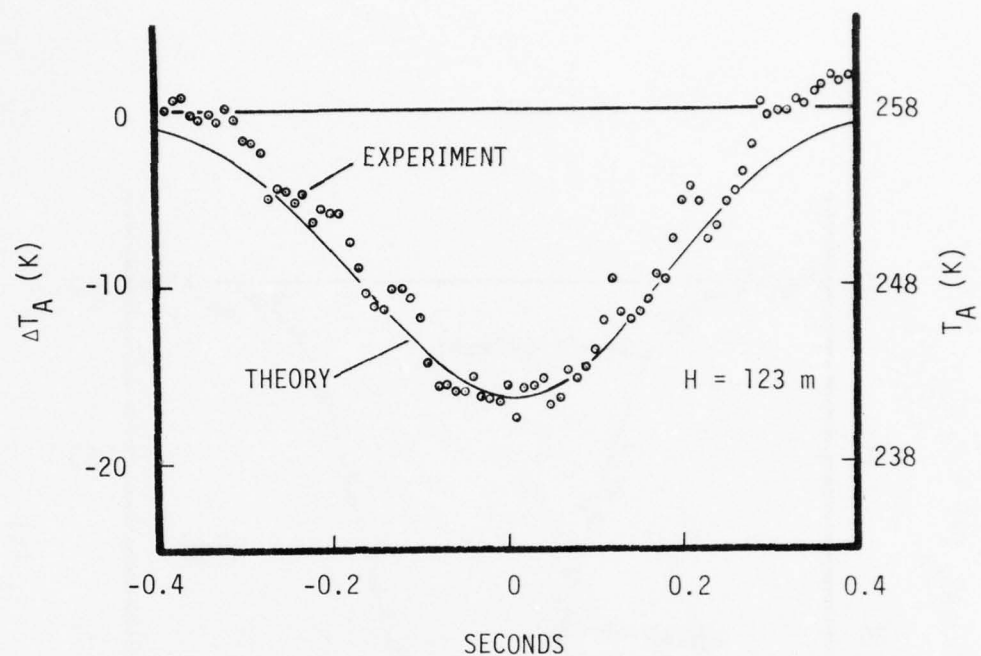Figure 8.   Radiometer Output, Run 11
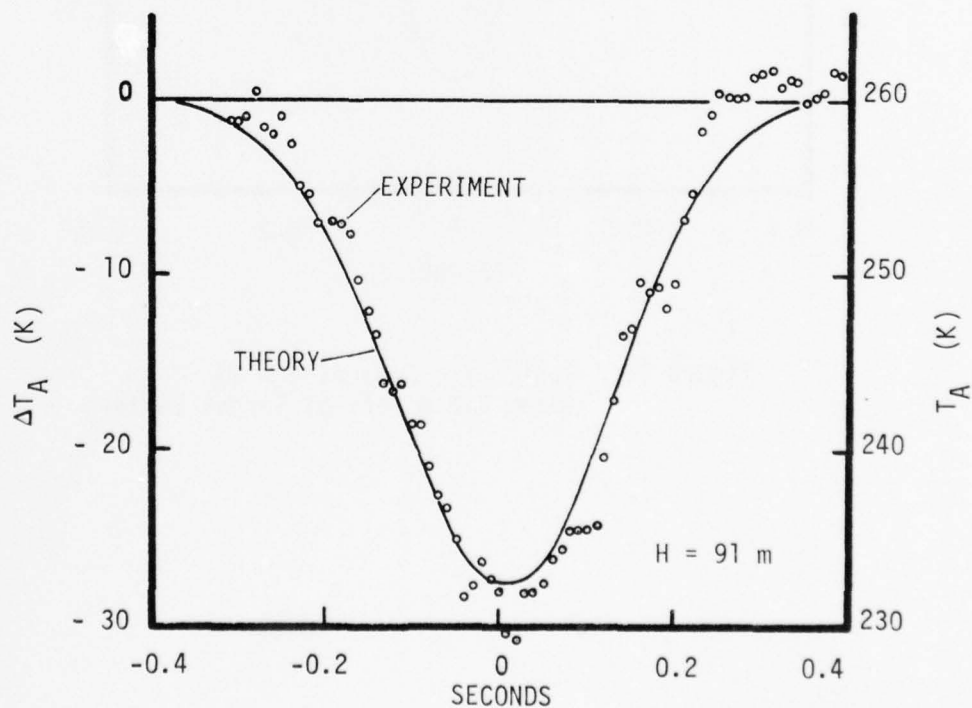(Beam 0.1 m Right of Target Center)

Figure 9.   Radiometer Output, Run 17
(Beam 1.1 m Left of Target Center)
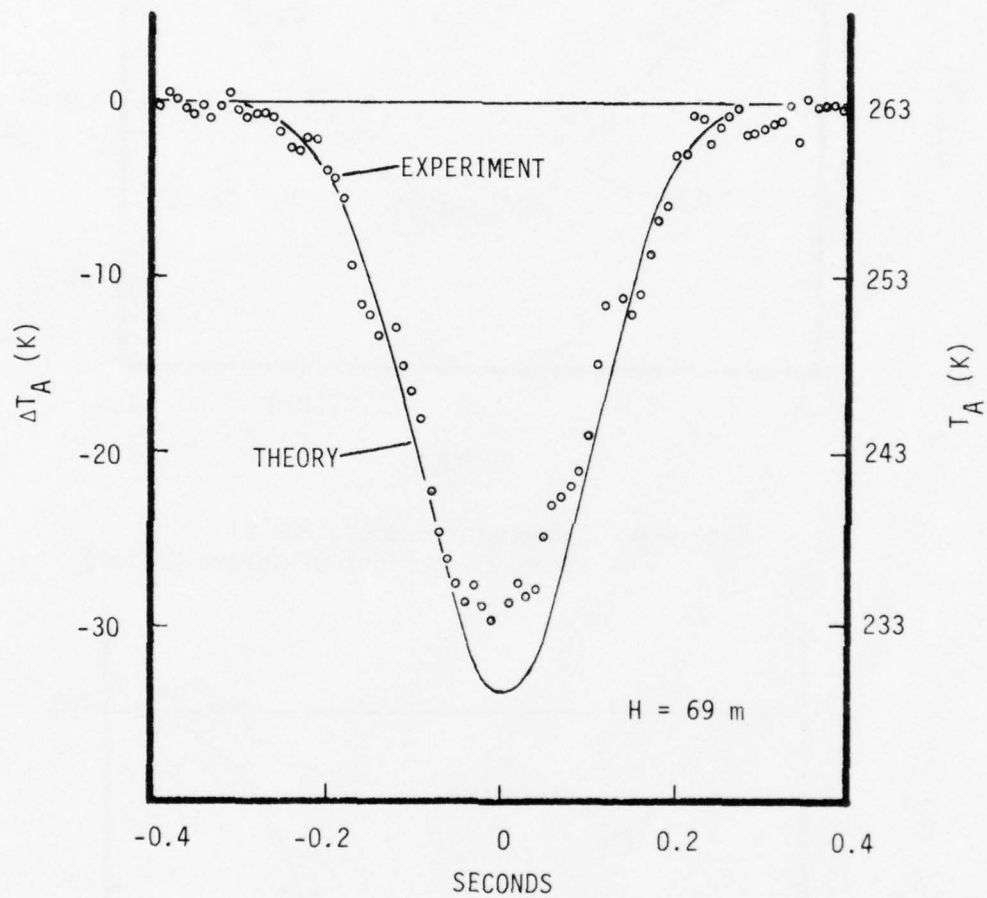
Figure 10.   Radiometer Output, Run 23
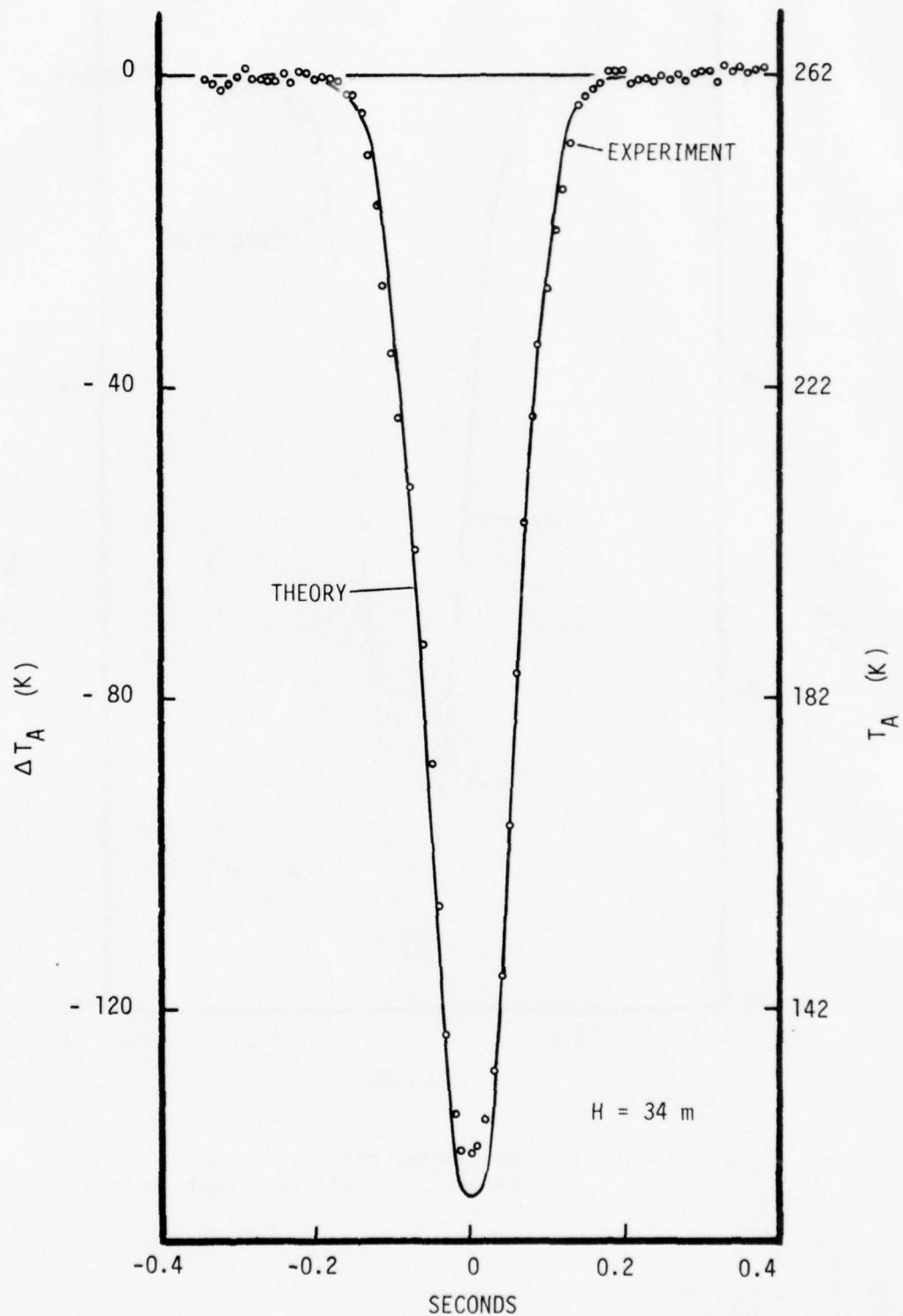   (Beam 2.6 m Left of Target Center)

Figure 11.   Radiometer Output, Run 26
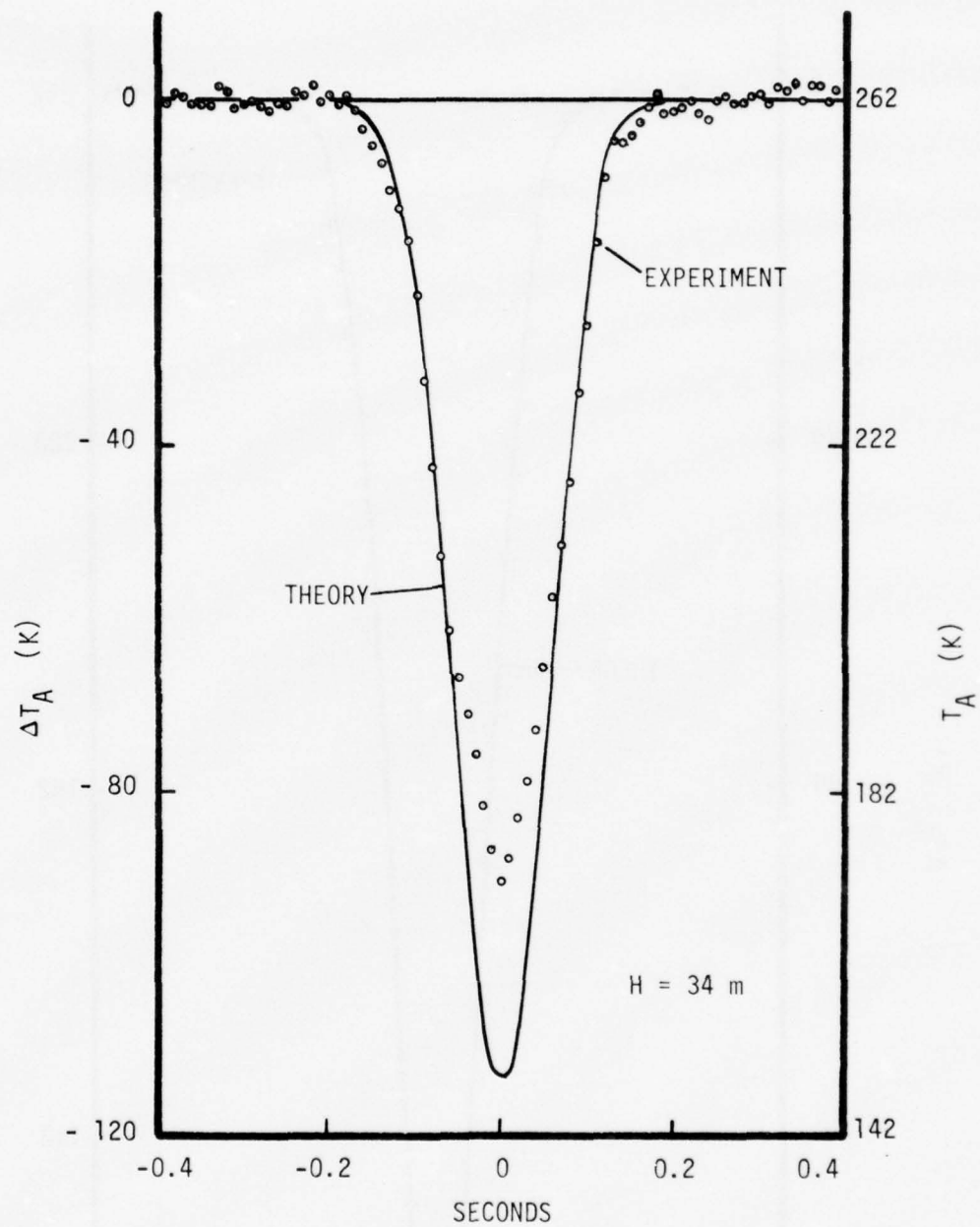   (Beam 0.1 m Left of Target Center)

Figure 12.   Radiometer Output, Run 25
            (Beam 1.3 m Left of Target Center)

30

oscillations of the helicopter at a frequency of about 10 Hz. Figure 9
shows results for an altitude of 91 m and the center of the antenna
beam passing about 1.1 m left of the center line of the target. Agree-
ment between theory and experiment is very good. Figure 10 shows
theoretical and experimental data for a case when the center of the
antenna beam was off the target (2.6 m to the left of target center)
as the helicopter passed over at an altitude of 69 m. Agreement is
generally good although the experimental values differ somewhat from
the theoretical values when the antenna beam is closest to the target.
Figure 11 shows the very high pulse obtained when the radiometer was
at an altitude of 34 m and was carried essentially over the center
line of the target. Agreement between theory and experiment is very
good although the experimental peak falls a bit short of the theoretical
peak. Small differences between theoretical and experimental results
would in part exist if actual experimental conditions differed from those
assumed. Knowledge of the target temperature contrast, the helicopter
speed and altitude, and the left-right position of the antenna beam is
not precise.

Almost all of the signal pulses obtained in the measurement program
agree as well with theory as those shown in Figures 8 through 11.
However, as mentioned above, two runs made at an altitude of 34 m,
and passing about 1.3 m from the center of the target did not produce
peak readings in line with theory. Figure 12 shows experimental and
theoretical data for one of these cases (Run 25). Agreement between
theory and experiment is good for the lower half of the signal pulse
($|\Delta T_A| < 55$ K) but the experiment values depart substantially from the
theoretical values near the peak of the pulse. The reason for the
discrepancy is not apparent. The experimental pulse has a somewhat
unusual shape; the possibility exists of some sort of problem during
this run. However, the video recording for this run shows nothing
unusual, and the unfiltered radiometer output (i.e., the radiometer
output prior to being passed through a 100-Hz filter) has the same
basic shape as the filtered signal pulse. Only this case and an almost
identical case (Run 27) produced experimental results differing
appreciably from theoretical results.

An estimate of the noise output of the radiometer was obtained for
each SADARM measurement run by calculating the standard deviation of the
digitized filtered data over a 0.2-second interval adjacent to the
signal pulse for the sheet metal target. Since the terrain at which the
radiometer was looking during these intervals was essentially uniform,
it follows that the short period variations in the radiometer output
were largely from radiometer noise. The standard deviations of these
variations constitute estimates of the root-mean-square value of the
noise. The values determined in this manner are tabulated with other
measured and calculated data in Appendix A. The average of the 26

31

values is 0.79 K, which is a little lower than the value of 0.94 K obtained from laboratory measurements on the radiometer (Reference 2).

A theoretical estimate of the radiometer noise is obtained from Taylor's expression as given in Section III:

$$\Delta T_{rms} = \frac{\sqrt{\pi}}{2} \left[\frac{(F-1)\ T_o + T_A}{\sqrt{B\tau}} \right] .$$

With the following values for the radiometer used in the measurement program,

$$F = 3.98 \ (6db)$$

$$T_o = 300 \ K$$

$$T_A = 260 \ K \ (typical)$$

$$B = 5 \times 10^8 \ Hz$$

$$\tau = 0.0025 \ sec,$$

the calculated value of ΔT_{rms} is 0.91 K. This value agrees well with the value from laboratory measurements.

The apparent signal-to-noise ratio for each measurement run was calculated by dividing the peak value of ΔT_A by the rms noise for that run. These S/N values are also tabulated in Appendix A. Comparison of these values with theoretical values can be made in several ways. For example, expression (B) for ΔT_A (derived in Section III) can be combined with Taylor's expression for noise to define the S/N ratio for cases when the antenna is pointing at the center of the target.

$$S/N = \frac{2\ (\Delta T_T/T_o) \left(1 - e^{-bA_T/\pi R^2}\right)\sqrt{B\tau}}{\sqrt{\pi}\ [(F-1) + T_A/T_o]} .$$

Using the numerical values given above, along with $\Delta T_T = 250 \ K$, $A_T = 11.59 \ m^2$ (projected area), and $b = 370$, results in $S/N = 273.3(1-e^{-1364.5/R^2})$. This function is plotted on Figure 13, along with experimental data for cases in which the radiometer pointed within 0.5 m of the center of the target. Agreement between experimental and theoretical values is good; it would be even better if the

32
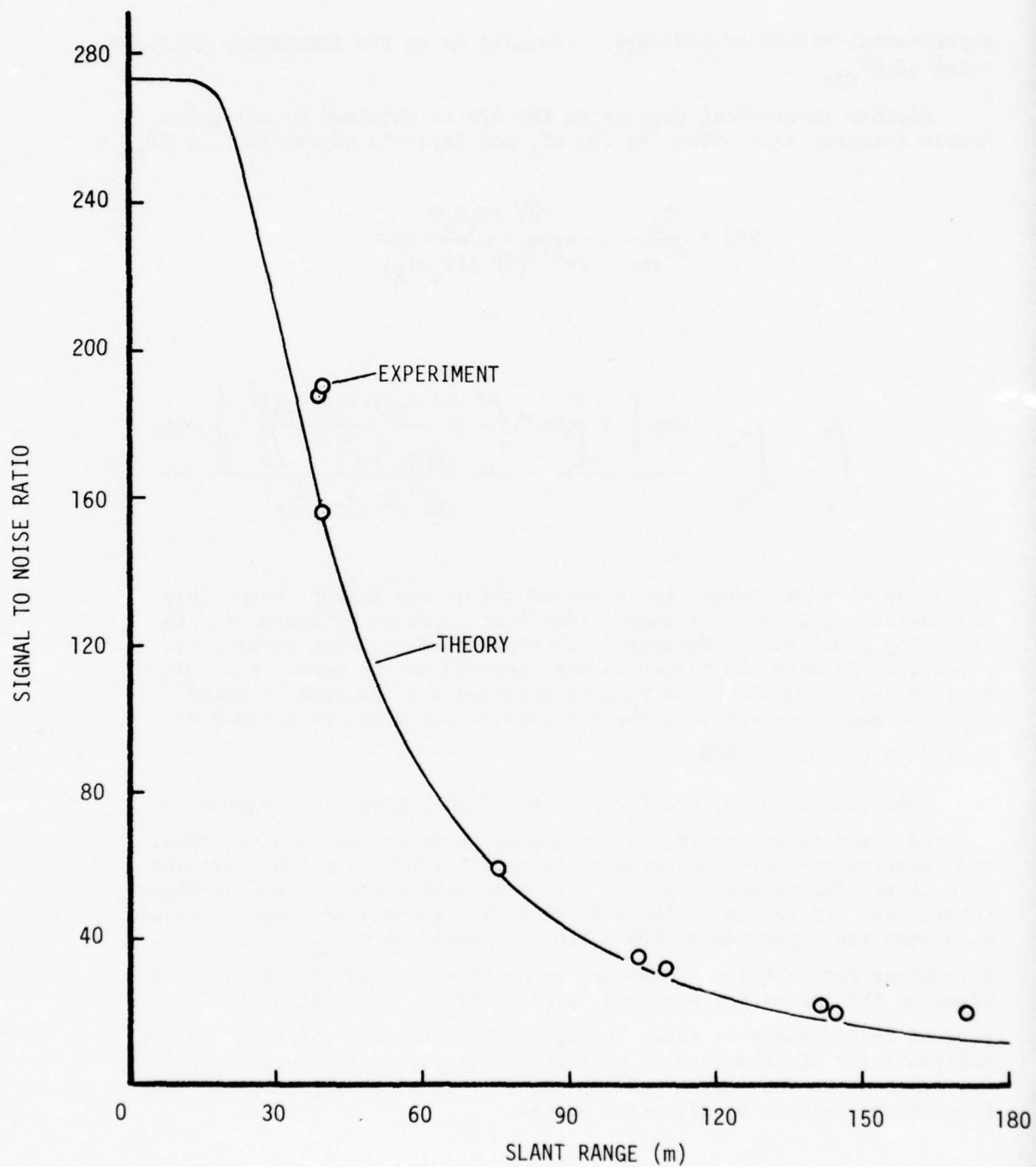
Figure 13. S/N vs Slant Range
(Beam Centered on Target)

experimental values of S/N were calculated using the laboratory measured value of ΔT_{rms}.

Another theoretical expression for S/N is obtained by using the double integral expression (A) for ΔT_A and Taylor's expression for ΔT_{rms}:

$$S/N = \frac{\Delta T_A}{\Delta T_{rms}} = \frac{\sqrt{B\tau}\ \Delta T_T G_o H}{2\pi^{3/2}[(F-1)T_o + T_A]}$$

$$x \quad \int_{y_1}^{y_2} \int_{x_1}^{x_2} \frac{\exp\left\{-b\left[\cos^{-1}\left(\frac{H\cos\theta_F + y\sin\theta_F}{(H^2+x^2+y^2)^{1/2}}\right)\right]^2\right\}dxdy}{(H^2+x^2+y^2)^{3/2}}.$$

For cases when the target is in the center of the antenna beam, this expression yields results almost identical to those obtained from the preceding expression. However, this expression can also be used to calculate S/N when the target is not centered in the beam. For numerical values cited above the results obtained are the same as shown for ΔT_A on Figure 7 except that the ordinate values would be divided by 0.91 K to convert to S/N.

Theoretical values of ΔT_A were read from Figure 7 for radiometer altitudes and target positions corresponding to the measurement runs, and these values were converted to theoretical S/N ratios by dividing by 0.91 K. The experimental S/N ratios were then plotted versus these theoretical S/N ratios. Figure 14 shows the general agreement obtained even when the experimental S/N ratios are based on ΔT_{rms} values as determined for each run. However, when the experimental S/N ratios are based on the laboratory measured value of ΔT_{rms}, the scatter in data is reduced considerably as shown by Figure 15. The only points which are substantially off the line of perfect correlation correspond to the two cases where the signal pulse peaks fell considerably short of the theoretical values, as discussed before.

34

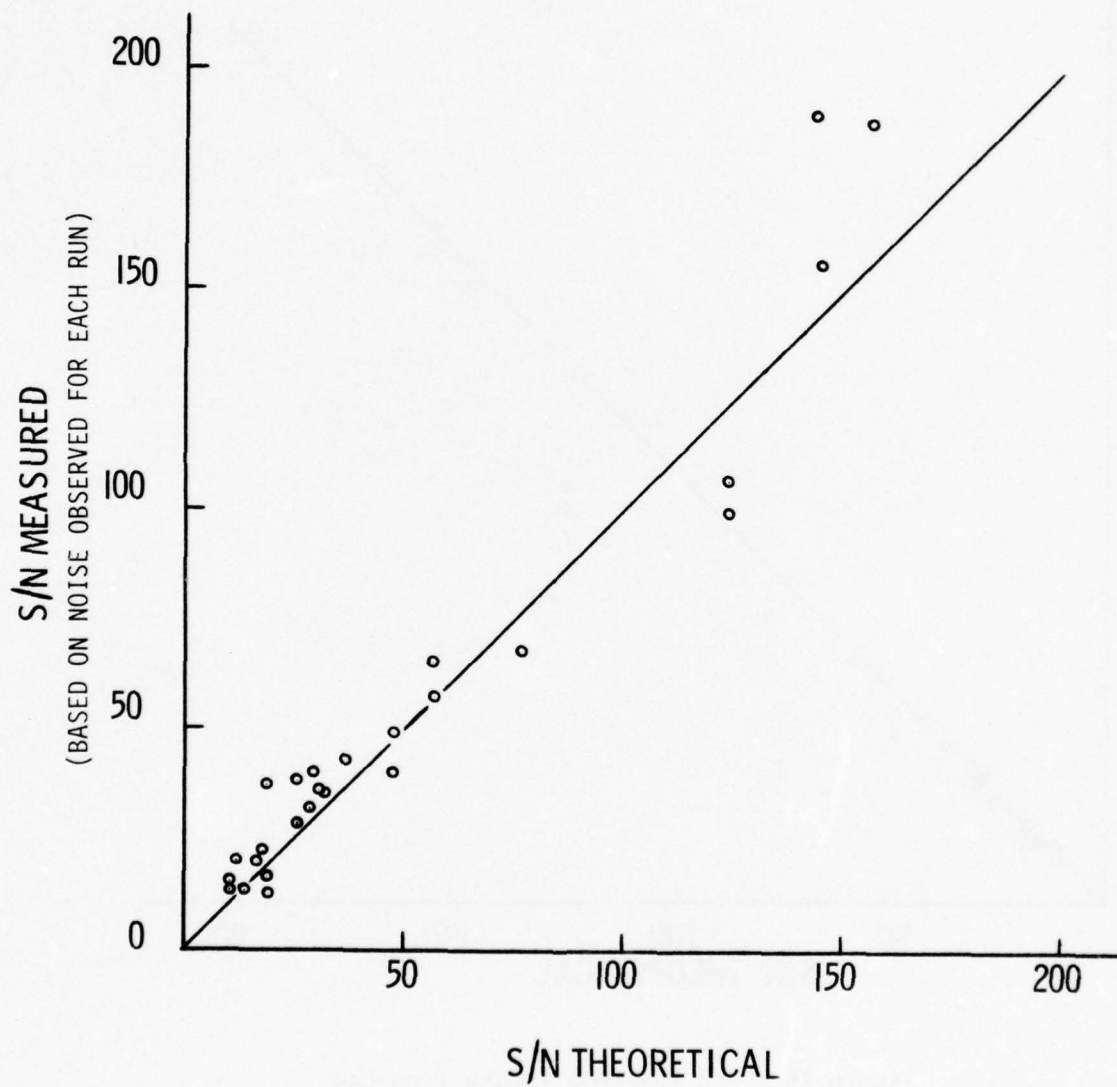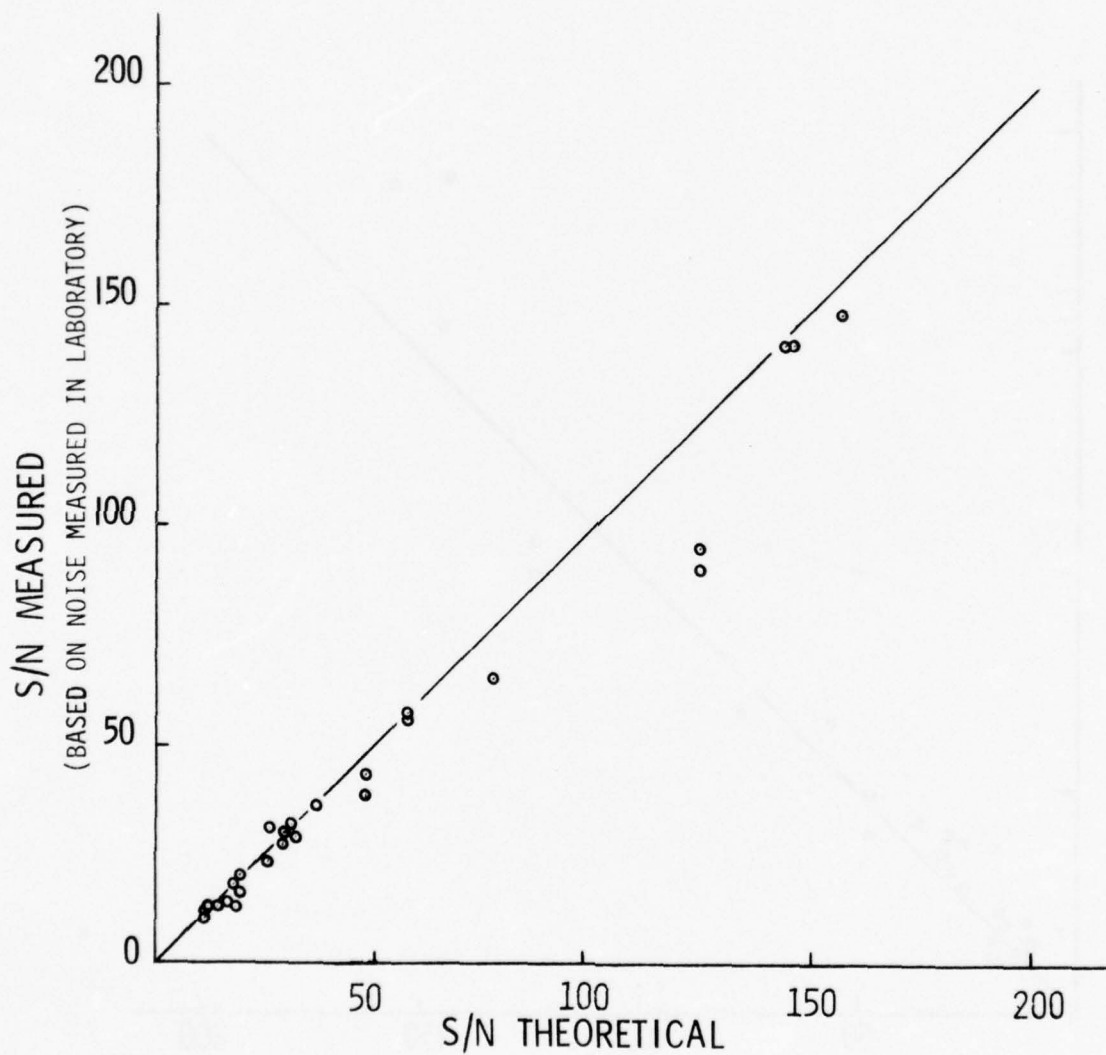Figure 14. S/N Measured (Observed Noise)
vs S/N Theoretical

35

Figure 15. S/N Measured (Noise from Lab
Measurement) vs S/N Theoretical

V.   SUMMARY AND CONCLUSIONS

Two expressions for calculating radiometer antenna temperature changes when a target is present were derived and compared with a simple expression frequently used in the literature. The new expressions yield good results even when the target is beam-filling whereas the frequently used expression does not. Moreover, the frequently used expression yields results which are too high by a factor of about $1/\ell n2$ even when the target does not fill the beam. One of the new expressions can be used to calculate the output signal of a radiometer as it passes over a target. The expression can be applied even when the radiometer does not pass directly over the target and when the radiometer antenna axis is tilted from the vertical.

Results from measurements made with a sheet metal target during the SADARM Measurement Program were used to check the theoretical expressions used in this study. Agreement between theory and experiment proved very good except for a few isolated cases. Both of the new expressions accurately predicted the experimental results (incremental radiometer readings) for cases when the radiometer passed over the center of the target. The second expression also predicted the off-center results quite well. A brief investigation of the effect of the change in sky reflection angle when the radiometer was not looking directly down on the target showed the effect to be small.

Theoretical signal pulses were calculated and compared with measured pulses. The amplitudes and shapes of the theoretical and experimental pulses were almost identical for most cases.

Radiometer noise outputs and signal-to-noise ratios were calculated theoretically and determined from SADARM measurement data. Noise levels determined from the radiometer outputs obtained during test runs and the S/N ratios computed using these noise values are in fair agreement with theory. When the radiometer noise output measured in the laboratory is used in the S/N computation for the experimental data, the agreement with theory is quite good.

Conclusions from this effort include the following:

1. A model has been developed which can be used to calculate the signal pulse from a passive radiometer when it passes over a flat target. Extension to more complex target shapes should be relatively straightforward, but not trivial.

2. Another model has been developed which can be used to calculate the peak signal change in the output of a radiometer when the target is centered in the radiometer antenna beam. This model is relatively simple but yields better results than an expression which is commonly used.

3. The accuracy of the models mentioned above has been verified using data from the SADARM Measurement Program.

4. Using Taylor's expression for the noise output of a radiometer, and the models mentioned above for the signal output of a radiometer, theoretical results have been obtained for S/N ratios which agree quite well with experimental values.

APPENDIX A

TABULATION OF DATA FROM SADARM MEASUREMENT PROGRAM

The SADARM (Sense and Destroy Armor) Measurement Program involved using a passive 35-GHz radiometer carried by helicopter over a line of targets consisting mostly of tanks but also including a square sheet of metal 3.66 m (12 ft) on a side. The basic data available were radiometer output in degrees Kelvin and helicopter altitude above ground in feet. Video recordings were made with a camera boresighted to the radiometer antenna axis, and time was recorded to enable synchronization of the data.

The data used in this study were taken on 26 March 1974, with a parabolic reflector antenna on the radiometer. Only data pertaining to the sheet metal target were used because analysis of performance of the radiometer is simpler for a two-dimensional target than for a complex three-dimensional one.

Thirty runs were made on 26 March 1974 but data were available for only 26. Table A-1 lists the basic information for each run, along with some processed data. The primary source of numerical values was a tabulation of radiometric temperature and altitude at 0.01-second intervals for each run. The temperature values were obtained by passing the output of the radiometer through a 100-Hz low-pass filter and digitizing the results. Computer-plotted signal pulses (antenna temperature versus time as the radiometer passed over the target) were also available for each run, but are not presented in this report.

Column 1 in the table identifies the run number. Column 2 gives the altitude as the helicopter passed over the metal sheet for that run, rounded to the nearest metre. Column 3 gives the scene temperature without the target, obtained by averaging the radiometer output readings over a 0.2-second interval (20 data points) adjacent to the signal pulse. These values were rounded to the nearest degree. Column 4 lists the minimum value of the radiometer output for each run. These values were deduced by looking at both the tabulations and the plots for each run and using judgment in removing radiometer noise and the effects of helicopter oscillations from the readings. Column 5 gives the differences between the values in columns 3 and 4. These values represent the peaks of the signal pulses; they are given as positive quantities even though the radiometer output drops as it passes over a metal target. Column 6 lists an estimate of the radiometer noise for each run. These values were obtained by calculating the standard deviation of the radiometer output over a 0.2-second interval (20 data points) adjacent to the signal pulse, and applying a small standard correction factor because of the finite sample size. Column 7 shows signal-to-noise ratio (S/N) obtained by dividing ΔT_A by T_{noise} for each run. Finally, column 8 shows the estimated position of the center of the antenna beam for each run. These estimates were obtained by viewing playbacks of the video tapes and noting the left-right position of the boresight spot when it was centered along the fore-aft dimension of the target.

41

A correction was applied to the estimated apparent position to account for a boresight error of approximately 10 mils (see Appendix B). A minus sign indicates that the beam was to the left of target center and a plus sign indicates that it passed to the right. An operator was attempting to keep the video camera centered (left-right) on the target as the helicopter passed over, by moving the XM21 gun mount to which the radiometer was attached. Because of the boresight bias, most passes were actually somewhat to the left of center.

TABLE A-1

1	2	3	4	5	6	7	8
RUN	ALT	T_s	T_{min}	ΔT_A	T_{noise}	S/N	Beam Position
	(m)	(K)	(K)	(K)	(K)		(m)
4	150	258	249	9	0.71	13	-2.6
5	153	258	247	11	0.72	15	-1.8
6	149	257	245	12	0.59	20	+0.4
7	126	257	240	17	0.87	20	-0.2
8	118	259	240	19	0.52	37	-0.8
9	121	259	243	16	0.72	22	-0.8
10	123	258	246	12	0.95	13	-3.2
11	123	259	242	17	0.79	22	+0.1
12	117	259	244	15	0.91	16	-2.0
13	90	259	229	30	0.83	36	-1.0
14	95	258	232	26	0.81	32	-0.5
15	81	259	225	34	0.80	43	-0.9
16	90	257	230	27	0.77	35	-0.4
17	91	260	232	28	0.70	40	-1.1
18	95	261	239	22	0.77	29	-2.0
19	64	259	205	54	0.83	65	+1.1
20	64	261	221	40	0.81	49	-2.0
21	66	260	207	53	0.90	59	+0.2
22	48	264	203	61	0.90	68	-1.5
23	69	263	234	29	0.77	38	-2.6
24	54	263	227	36	0.91	40	-2.4
25	34	262	173	89	0.83	107	-1.3
26	34	262	123	139	0.74	188	-0.1
27	34	261	176	85	0.86	99	-1.3
28	35	261	128	133	0.70	190	+0.5
29	35	260	127	133	0.85	156	+0.2

43

APPENDIX B

DETERMINATION OF ANTENNA GAIN PATTERN PARAMETER b

In the text of this report the radiometer antenna gain pattern was assumed to be of the form

$$G(\theta) = G_o e^{-b\theta^2} .$$

Using this expression, a relationship was derived for the peak change in radiometer output:

$$\Delta T_A / \Delta T_T = \left(1 - e^{-bA_T/\pi R^2}\right) .$$

In this expression A_T is the projected area of a target which is at a range R from the radiometer, ΔT_A is the peak change in temperature as indicated by the radiometer and ΔT_T is the temperature contrast of the target with respect to its background. The target is assumed to be in the center of the antenna pattern.

Solving for b yields

$$b = -\frac{\pi R^2}{A_T} \ell n \left(1 - \Delta T_A / \Delta T_T\right) .$$

Thus, data obtained in the SADARM Measurement Program can be used to find a value for b.

The slant range R for each run was obtained by dividing the altitude (tabulated in Appendix A) by cos 30° to account for the tilt angle of the radiometer antenna. The projected area of the sheet metal target as seen by the radiometer was 11.59 m^2. It was assumed that the terrain had a radiometric temperature of 271 K and the sky radiometric temperature was 21 K. These values were based on radiometer measurements adjusted for backlobe effects. The target contrast was therefore about 250 K. The value of ΔT_A for each run is given in Appendix A.

Using the numerical values described above, b was determined for each measurement run. Results are listed in Table B-1. Ideally, if the target was centered in the antenna beam, and the values of ΔT_A, ΔT_T, and R were correct, b would be about the same for all runs. In reality, the target was not centered in all cases, and there is uncertainty regarding values of ΔT_A, ΔT_T and R.

47

TABLE B-1

RUN	b	BORESIGHT POSITION (FT)	(MILS)
4	297	3 left	(-5.3)
5	382	0	(0)
6	394	7 right	(+12.4)
7	407	4 "	(+9.0)
8	396	2 "	(+4.5)
9	346	2 "	(+4.4)
10	265	6 left	(-13.0)
11	385	5 right	(+10.7)
12	306	2 left	(-4.5)
13	368	0	(0)
14	360	2 right	(+5.5)
15	350	0	(0)
16	335	2 right	(+5.9)
17	362	0	(0)
18	297	3 left	(-8.4)
19	261	6 right	(+24.7)
20	259	4 left	(-16.5)
21	383	3 right	(+11.9)
22	229	3 left	(-16.6)
23	214	6 "	(-22.9)
24	162	6 "	(-29.5)
25	191	3 "	(-22.9)
26	335	1 right	(+7.8)
27	171	3 left	(-23.4)
28	346	3 right	(+22.3)
29	329	2 "	(+15.2)

The video tapes of the runs were viewed and estimates were made of the apparent left-right position of the boresight when it was centered on the fore-aft dimension of the target. These estimates are listed in Table B-1. The values are in feet because the estimates were relative to the size of the target, which is 12 feet (3.66 m) on a side. A plot of b versus boresight position (Figure B-1) shows a definite trend toward higher b values when the boresight was somewhat to the right of target center. It seems reasonably clear that there was a boresight bias between the video camera and the radiometer antenna.

(The scatter in points on Figure B-1 is quite readily explained by the high sensitivity of b to ΔT_A when R is relatively large (e.g., 25/K for conditions of run 7), and to R when R is relatively small (e.g., 17/m for conditions of run 26). Further, the readings of boresight position were fairly crude.)

If the boresight left-right position is converted to an equivalent pointing error, the values in parentheses in Table B-1 are obtained. Then, when b is plotted versus the equivalent pointing error (Figure B-2) it appears that b maximizes at a boresight angle of roughly 10 mils. This value is assumed to represent an error in boresighting the video camera to the radiometer antenna. The apparent boresight position (i.e., the apparent left-right position of the radiometer as it was carried over the target) for each run was adjusted to the value given in Appendix A, based on this boresight error.

The value of b which characterizes the radiometer antenna pattern was selected as 370 from Figure B-2. The peak gain of the antenna is then 370 x 4 = 1480 or 31.7 db. This value agrees quite well with the value of 32 db quoted for this antenna (measured with 35-GHz coherent radiation). The 3-db beamwidth is computed to be

$$2(\ln2/b)^{1/2} \text{ rad} = 2(\ln2/370)^{1/2} = 0.0866 \text{ rad} = 4.96 \text{ deg},$$

compared with about 4 degrees measured with coherent radiation.

Figure B-1. Apparent Value of b vs Boresight Position

APPARENT VALUE OF b

400

300

200

100

0

-6   -3   0   3   6

LEFT   RIGHT
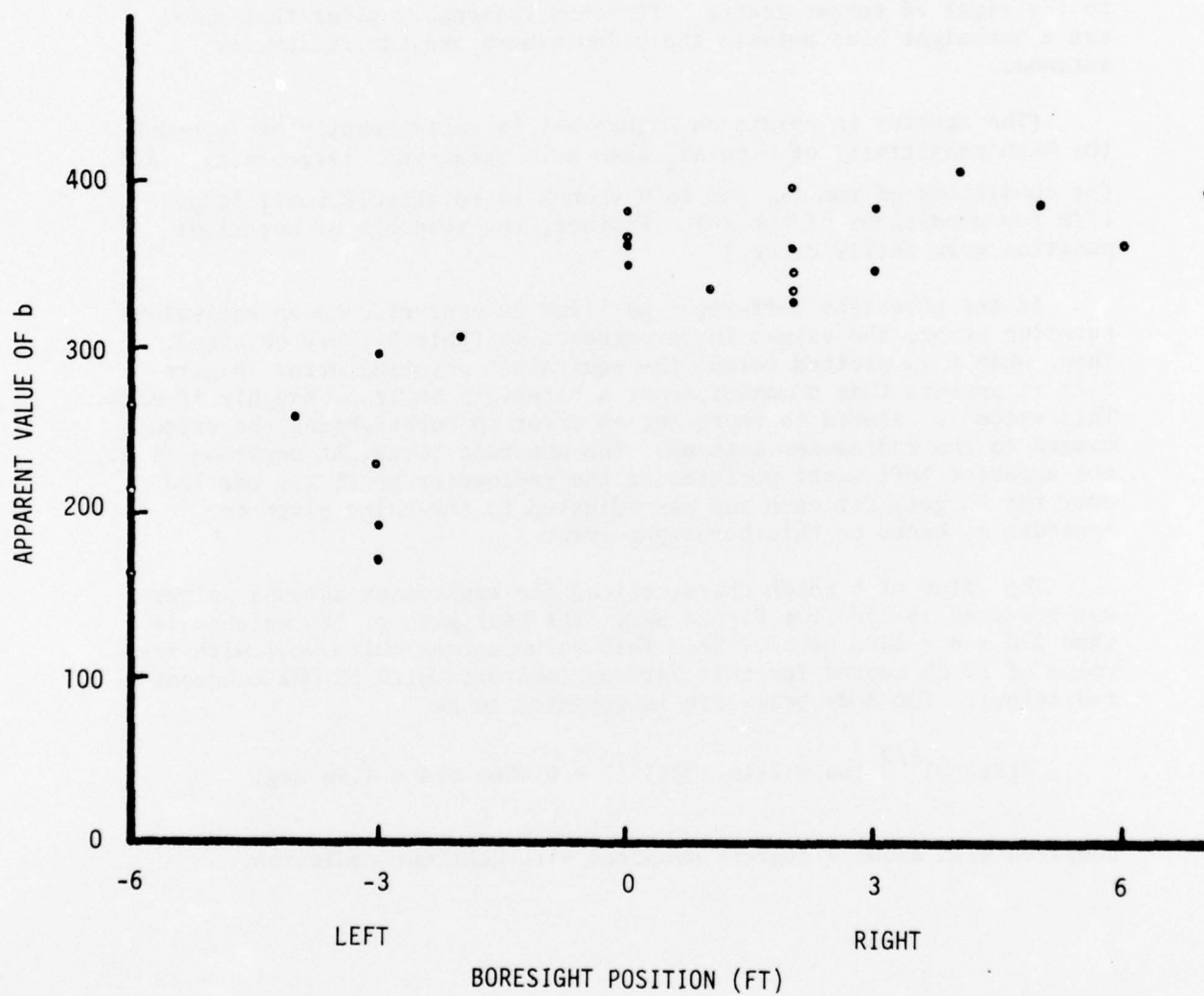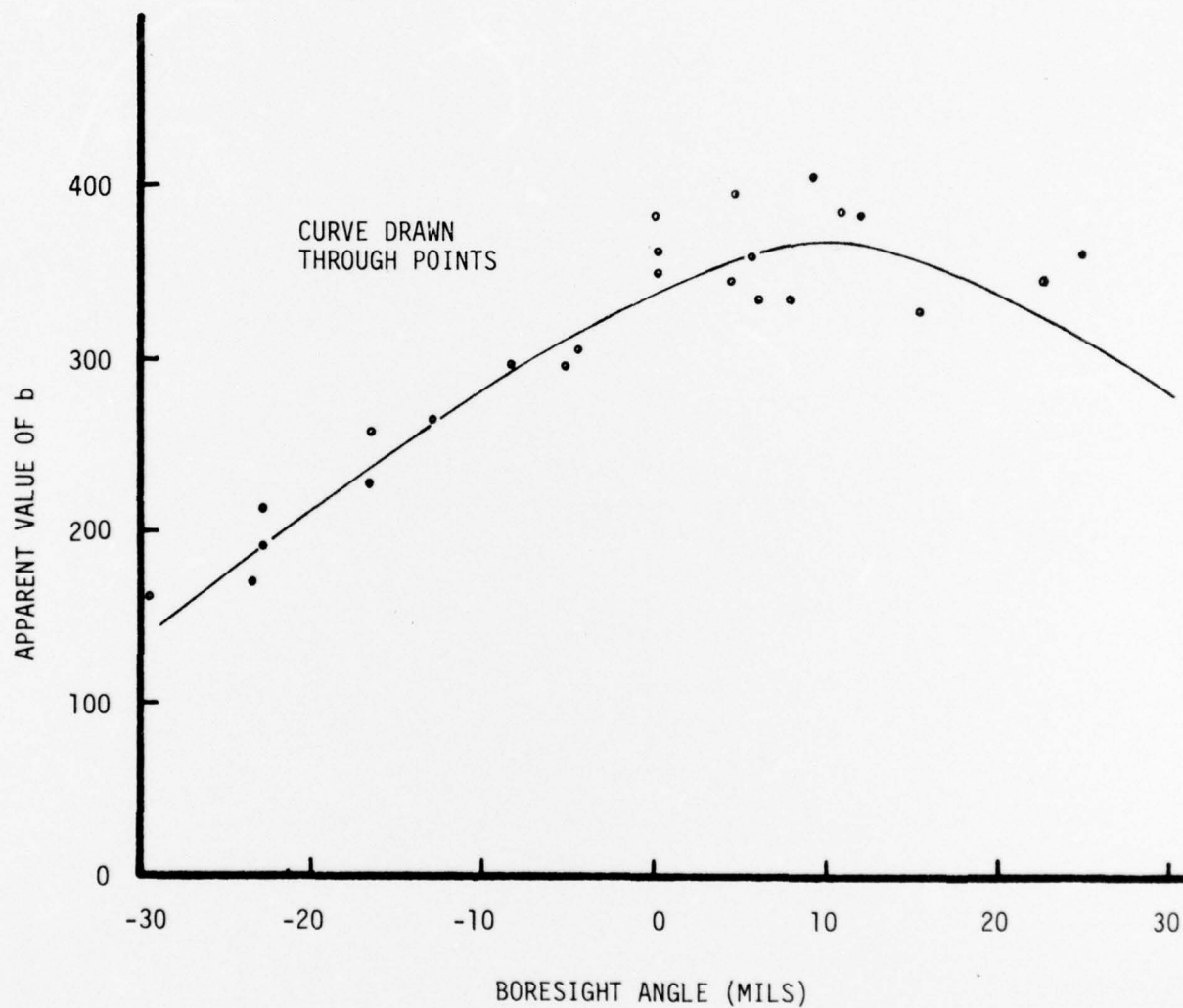
BORESIGHT POSITION (FT)

Figure B-2. Apparent Value of b vs Boresight Angle

APPENDIX C

THE EFFECT OF RADIOMETRIC SKY TEMPERATURES AWAY FROM ZENITH

Implicit in the expression derived in Section III for calculation of the output signal of a radiometer, viz.

$$\Delta T_A = \frac{\Delta T_T G_o H}{4\pi} \int_{y_1}^{y_2} \int_{x_1}^{x_2} \frac{\exp\left\{-b\left[\cos^{-1}\left(\frac{H\cos\theta_F + y\sin\theta_F}{[H^2+x^2+y^2]^{1/2}}\right)\right]^2\right\} dxdy}{\left(H^2+x^2+y^2\right)^{3/2}} ,$$

is the assumption that the target temperature relative to its background, ΔT_T, is constant regardless of the angle between the axis of the antenna and the target. Actually, if the radiometer is looking essentially straight down on a horizontal reflective metal target, the target appears to have the temperature of the zenith sky, and if the radiometer is viewing the target at an angle the apparent temperature of the target will be that of some part of the sky away from the zenith. However, as is shown by the plot of typical data for a 35-GHz radiometer (Figure C-1), the apparent sky temperature does not increase much until the zenith angle exceeds roughly 40°. Thus, even though the antenna in the SADARM tests was tilted 30° forward, i.e., its axis was 30° from the vertical, it did not appear likely that the effect from seeing non-zenith sky temperatures would be very great. Nevertheless, when some of the theoretical results for cases when the radiometer did not pass directly over the center of the target came out a bit higher than the measured results, it appeared appropriate to make a quantitative check.

If the data shown on Figure C-1 are replotted in terms of $\Delta T_T(\alpha)/\Delta T_T(o)$, which is the target temperature normalized relative to the contrast when viewed from directly overhead, the plot is as shown in Figure C-2. A good fit to this curve is obtained using the form

$$\Delta T_T(\alpha) \Big/ \Delta T_T(o) = 1 - k_1 e^{k_2 \alpha} ,$$

where k_1 and k_2 are positive constants and α is the zenith angle given by

$$\alpha = \tan^{-1} \frac{(x^2 + y^2)^{1/2}}{H} \quad \text{rad}$$
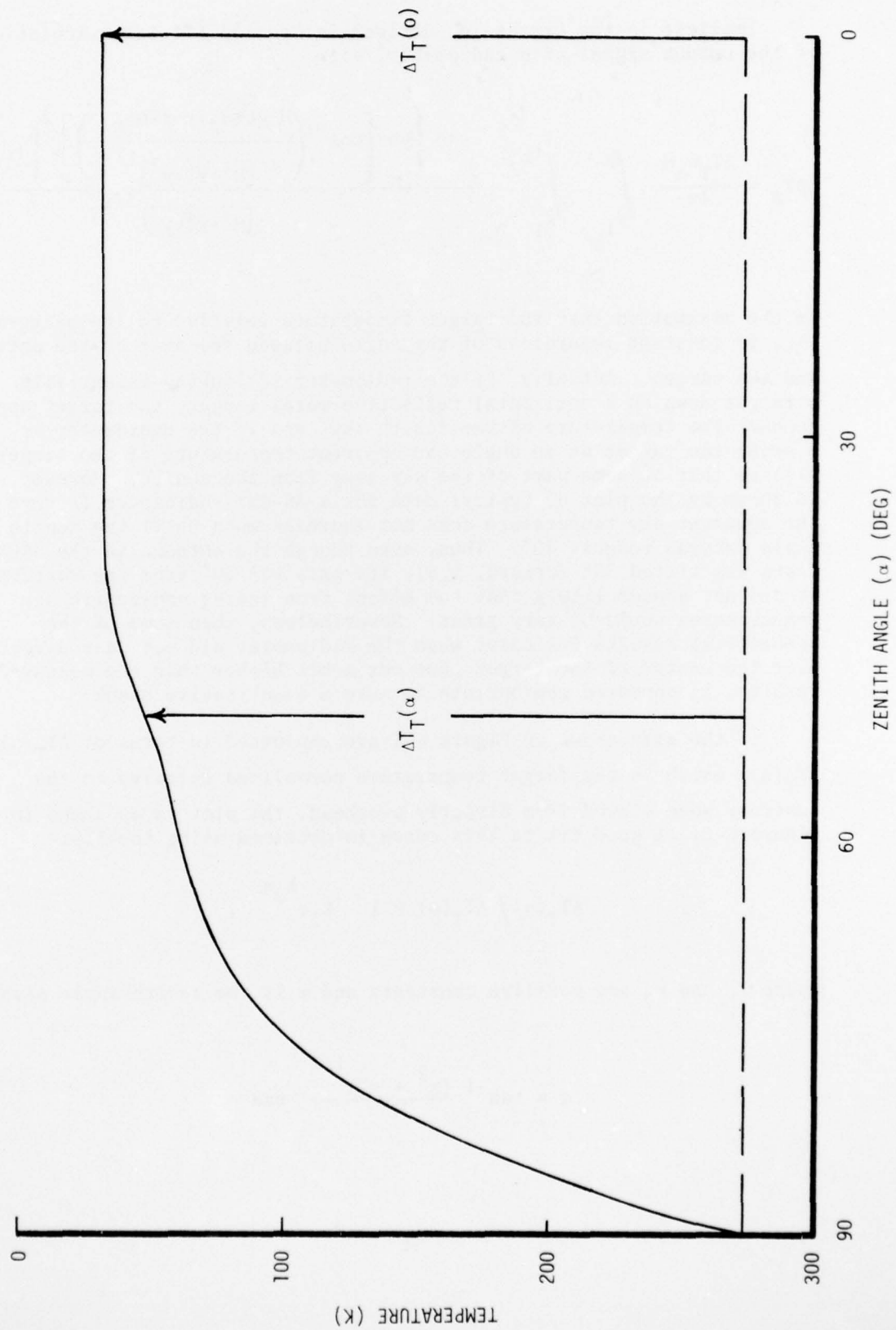
55

Figure C-1. Radiometric Sky Temperature at 35 GHz (Typical)

$1 - 0.001 \, e^{4.398\alpha} \, (\text{RAD})$

FROM 35 GHz DATA

ZENITH ANGLE (α) (DEG)

$\Delta T_T(\alpha)/\Delta T_T(0)$

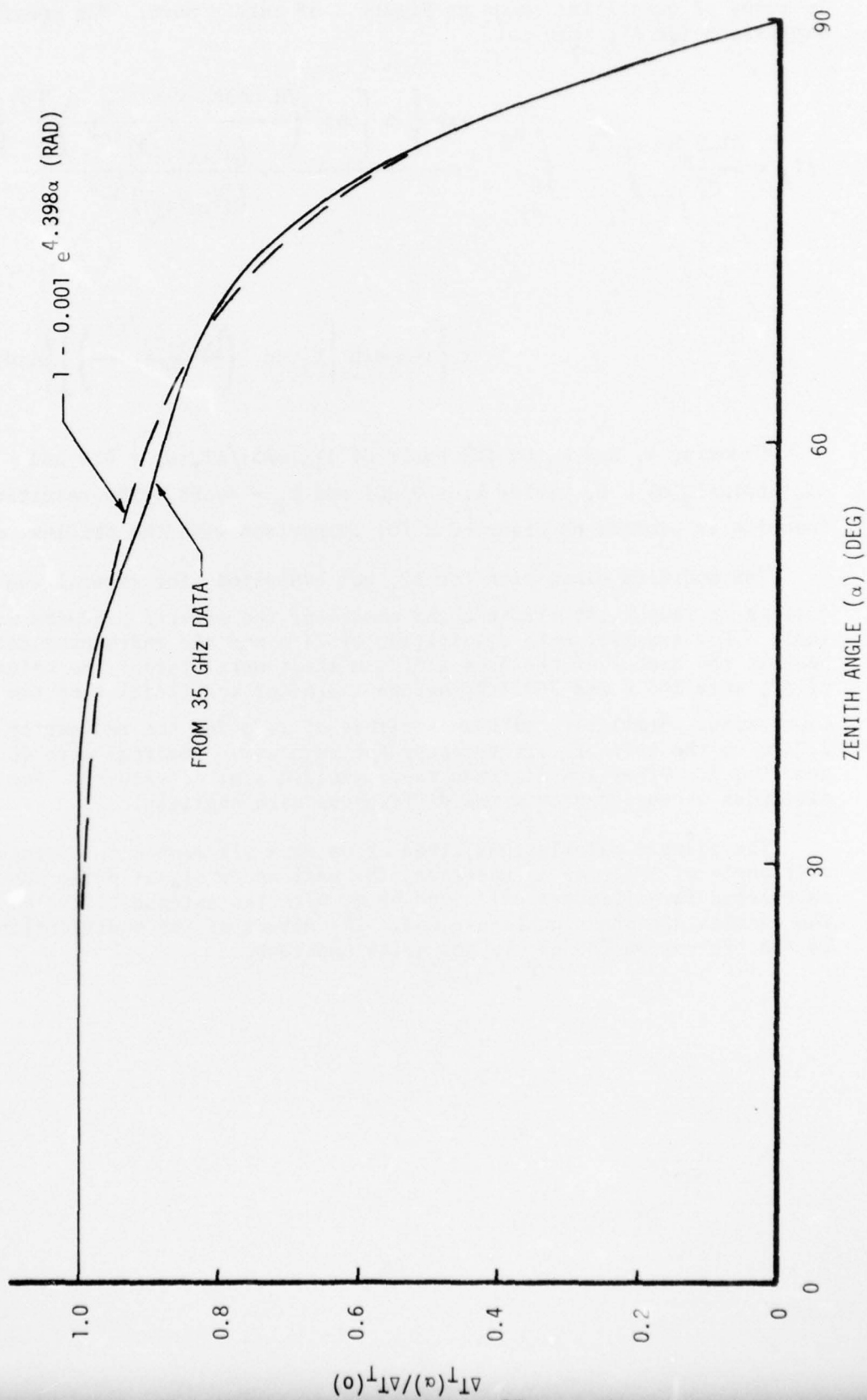Figure C-2. Relative Target Contrast

in terms of quantities shown on Figure 3 of this report. The modified
expression for ΔT_A then is

$$\Delta T_A = \frac{\Delta T_T G_o H}{4\pi} \int_{y_1}^{y_2} \int_{x_1}^{x_2} \frac{\exp\left\{-b\left[\cos^{-1}\left(\frac{H\cos\theta_F + y\sin\theta_F}{[H^2+x^2+y^2]^{1/2}}\right)\right]^2\right\}}{(H^2+x^2+y^2)^{3/2}}$$

$$x\left\{1-k_1\exp\left[k_2\tan^{-1}\left(\frac{(x^2+y^2)^{1/2}}{H}\right)\right]\right\}dxdy$$

Choosing k_1 and k_2 on the basis of $\Delta T_T(\pi/3)/\Delta T_T(o) = 0.9$ and
$\Delta T_T(\pi/2)/\Delta T_T(o) = 0$, yields $k_1 = 0.001$ and $k_2 = 4.398$. The resulting
function is plotted on Figure C-2 for comparison with the original data.

The modified expression for ΔT_A was evaluated for several con-
ditions of radiometer altitude and position; the effects produced were
small. For example, with an altitude of 24 m and the radiometer antenna
beam at the center of the 3.66 x 3.66 m sheet metal target the values
of ΔT_A were 203.8 and 202.3 K, before and after modification of the
expression. Similarly, with an altitude of 24 m and the radiometer
2.74 m to the left of target center the respective readings were 40.5
and 40.2 K. Other low altitude cases yielded similar results. For
altitudes above about 30 m the differences were negligible.

The example calculations cited above were all made with an antenna
tilt angle of 30°. As an exercise, the radiometer signal pulse was
calculated for altitudes of 34 and 68 m, with the antenna tilted 60°.
The results are shown on Figure C-3. The effect of the modification
to the expression for ΔT_A is now quite apparent.
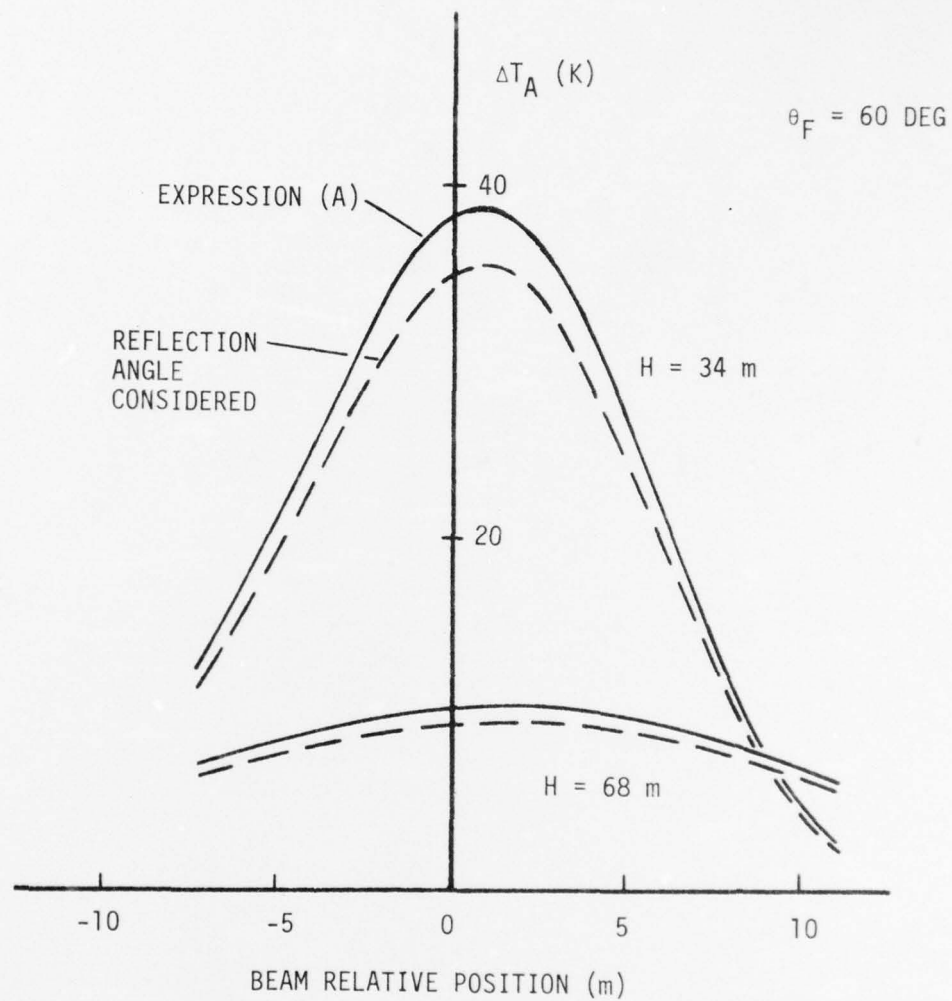
58

Figure C-3. Effect of Sky Reflection Angle on
Radiometer Signal Pulse

DISTRIBUTION LIST

No. of Copies	Organization	No. of Copies	Organization
12	Commander Defense Documentation Center ATTN: DDC-TCA Cameron Station Alexandria, VA 22314	1	Director US Army Air Mobility Research and Development Laboratory Ames Research Center Moffett Field, CA 94035

2	Director of Defense Research
	    and Engineering
	Engineering Technology
	ATTN: Mr. L. Weisberg
	        Dr. D. Charvonia
	Washington, DC 20301
		4	Commander
			US Army Electronics Command
			ATTN: DRSEL-RD
			        DRSEL-CT
			        DRSEL-CT-R, Mr. Pearce
			        DRSEL-VL, Mr. Post
			Fort Monmouth, NJ 07703

1	Director
	Defense Advanced Research
	    Projects Agency
	ATTN: Dr. J. Tegnelia
	1400 Wilson Boulevard
	Arlington, VA 22209
		1	Office of the Test Director
			Joint Services LGW/CM Test
			    Program
			ATTN: DRSEL-WL-MT, R. Murray
			White Sands Missile Range
			NM 88002

1	Director Institute for Defense Analyses 400 Army Navy Drive Arlington, VA 22202	1	Commander US Army Electronics Command Atmospheric Science Research ATTN: DRSEL-BL-RD Fort Huachuca, AZ 85613
1	Director Defense Nuclear Agency ATTN: STRA (RAEL), LTC Brown Washington, DC 20305	1	Director US Army Night Vision Laboratory Visionics Technical Area ATTN: DRSEL-NV-VI, J.R. Moulton Fort Belvoir, VA 22060

1	Commander
	US Army Materiel Development
	    and Readiness Command
	ATTN: DRCDMA-ST
	5001 Eisenhower Avenue
	Alexandria, VA 22333
		4	Commander
			US Army Missile Research
			    and Development Command
			ATTN: DRDMI-R, Mr. Pittman
			        DRDMI-RBL
			        DRDMI-RES
			        DRDMI-RER, Mr. H. Green
			Redstone Arsenal, AL 35809

1	Commander US Army Aviation Systems Cmd ATTN: DRSAV-E 12th and Spruce Streets St. Louis, MO 63166		

DISTRIBUTION LIST

No. of Copies	Organization	No. of Copies	Organization
3	Commander US Army Missile Research and Development Command ATTN: DRDMI-RF, Mr. C. Hussey DRDMI-RFC, A. Michetti DRDMI-RFE, Mr. Salonimer and Mr. Duvall Redstone Arsenal, AL 35809	4	Commander US Army Frankford Arsenal ATTN: DRDAR-SCF (2 cys) Mr. R. Phielsticker Mr. J. Schmitz Mr. S. Greenberg Philadelphia, PA 19137
1	Commander US Army Missile Research and Development Command Redstone Scientific Info Center ATTN: Chief, Document Station Redstone Arsenal, AL 35809	1	Commander US Army Armament Research and Development Command ATTN: DRDAR-LCV-DE, T. Malgeri Dover, NJ 07801
1	Commander US Army Tank Automotive Development Command ATTN: DRDTA-RWL Warren, MI 48090	1	Commander US Army White Sands Missile Range ATTN: STEWS-TE, J. Flores White Sands, NM 88002
3	Commander US Army Mobility Equipment Research & Development Command ATTN: DRSME-RZT SMEFB-EM, K. Steinback Tech Docu Cen, Bldg. 315 Fort Belvoir, VA 22060	2	Commander US Army Harry Diamond Labs ATTN: DRXDO-TI DRXDO-RA, J. Salerno 2800 Powder Mill Road Adelphi, MD 20783
1	Commander US Army Armament Materiel Readiness Command Rock Island, IL 61202	1	Commander US Army Foreign Science and Technology Center Federal Office Building 220 7th Street Charlottesville, VA 22901
1	Commander US Army Armament Research and Development Command ATTN: DRDAR-SE, J. Brinkman Dover, NJ 07801	1	Commander US Army Training and Doctrine Command Fort Monroe, VA 23351
1	Director US Army Rock Island Arsenal ATTN: DRDAR-GSR Rodman Laboratory Rock Island, IL 61202	1	Director US Army TRADOC Systems Analysis Activity ATTN: ATAA-SA White Sands Missile Range NM 88002

DISTRIBUTION LIST

No. of Copies	Organization	No. of Copies	Organization
1	Commander US Army Combined Arms Combat Development Activity Fort Leavenworth, KS 66027	1	Commander Center for Naval Analyses ATTN: Document Control 1401 Wilson Boulevard Arlington, VA 22209

1	Office of Assistant Secretary
	  of the Army for R&D
	Assistant for Electronics
	ATTN: Mr. Victor L. Friedrich
	Washington, DC 20310
		2	Commander
			US Naval Air Development Center
			ATTN: AETD, Radar Division
			        Mr. M. Foral
			Warminster, PA 18974

1	HQDA (DAMA-CSM-CA, LTC Conner) Washington, DC 20310	2	Commander US Naval Electronics Lab Ctr ATTN: Code 2330, J.H.Provencher Tech Library San Diego, CA 92152
1	HQDA (DAMA-DDZ-C) Washington, DC 20310		
1	Commander US Army Research Office ATTN: Dr. D. Van Hulsteyn P. O. Box 12211 Research Triangle Park, NC 27709	2	Commander US Naval Surface Weapons Center ATTN: Library Code DF34 Dahlgren, VA 22448

1	Commander
	TCTA
	ATTN: Scientific Advisor
	Fort Hood, TX 76544
		3	Commander
			US Naval Weapons Center
			ATTN: Mr. R. Moore
			        Mr. R. Higuera
			        Dr. J. Battles, Code 6014
			China Lake, CA 93555

1	Commander
	US Army Research and
	  Development Group (Europe)
	ATTN: Electronics Branch
	Box 15
	FPO New York 09510
		2	Director
			US Naval Research Laboratory
			ATTN: Code 5370, Radar
			        Geophysics Branch
			        Code 5460, Electro-
			        magnetic Prop Branch
			Washington, DC 20375

1	Commander US Naval Air Systems Command ATTN: AIR-2324, Mr. C. Francis Washington, DC 20360	1	AFATL/DLB Eglin AFB, FL 32542
1	Chief of Naval Research Department of the Navy Washington, DC 20360	1	AFATL/DLTG, F.H. Prestwood Eglin AFB, FL 32542

DISTRIBUTION LIST

No. of Copies	Organization	No. of Copies	Organization
2	AFATL (DLY/DLDG) Eglin AFB, FL 32542	1	Hughes Aircraft Company Aerospace Group Radar Division ATTN: Dr. R. Wagner Culver City, CA 90230
1	ADTC/ADBPS-12 Eglin AFB, FL 32542		
1	ADTC/ADA Eglin AFB, FL 32542	2	Hughes Aircraft Company Aerospace Group Electron Dynamic Division ATTN: Mr. N. B. Kramer Mr. J. F. Sparacio 3100 West Lomita Boulevard Torrance, CA 90504
1	RADC/EMATE Griffiss AFB, NY 13440		
2	AFGL (LZ, Mr. C. Sletten; LZN, E.E. Altschuler) Hanscom AFB, MA 01731		
1	AFWL/DEV Kirtland AFB, NM 87117	1	LTV Aerospace Corporation Michigan Division ATTN: Dr. J. Mayersak P. O. Box 909 Warren, MI 48090
1	AFAL/WRP, Mr. Leasure Wright-Patterson AFB, OH 45433	1	Martin Marietta Corporation ATTN: Dr. Jim Wiltse P. O. Box 5837 Orlando, FL 32805
1	AFAL (RWN-1, Mr. Ray Bruns) Wright-Patterson AFB, OH 45433		
1	AFWL/TEM-4, CPT J. Schell Wright-Patterson AFB, OH 45433	1	The Rand Corporation ATTN: Dr. S.J. Dudzinsky, Jr. 1700 Main Street Santa Monica, CA 90406
1	Goodyear Aerospace Corporation Arizona Division ATTN: Mr. Fred Wilcox Litchfield Park, AZ 85340	1	Raytheon Company Missiles Systems Division ATTN: Mr. Walter Justice Hartwell Road Bedford, MA 01730
1	Honeywell, Inc. Systems and Research Division ATTN: Mr. C. Seashore 2700 Ridgway Parkway Minneapolis, MN 55413		
		1	Sperry Rand Corporation Microwave Electronics Division ATTN: Mr. R. Roder Clearwater, FL 33518
1	Hughes Aircraft Company Aerospace Group Advanced Program Development Systems Division ATTN: P. B. Reggie Canoga Park, CA 91304		

DISTRIBUTION LIST